Title: Wetter Winters, Drier Summers: Quantifying the change in hydrological response around the Puget Sound area using the wflow_sbm hydrological model and CMIP6 projections

Authors: Joost Buitink[1], Brendan Dalmijn[2], Kai A. Parker[3], Kees Nederhoff[4], and Eric Grossman[5]

1: Deltares. (joost.buitink@deltares.nl)
2: Deltares. (brendan.dalmijn@deltares.nl)
3: U.S. Geological Survey. (kaparker@usgs.gov)
4: Deltares USA. (kees.nederhoff@deltares-usa.us)
5: U.S. Geological Survey. (egrossman@usgs.gov)

Wetter Winters, Drier Summers: Quantifying the change in hydrological response around the Puget Sound area using the wflow_sbm hydrological model and CMIP6 projections

Joost Buitink[1], Brendan Dalmijn[1], Kai A. Parker[2], Kees Nederhoff[3], and Eric Grossman[2]

[1]Deltares, Boussinesqweg 1, Delft, 2629 HV, the Netherlands
[2]U.S. Geological Survey, Pacific Coastal and Marine Science Center, Santa Cruz, CA, USA
[3]Deltares USA, 8601 Georgia Ave, Silver Spring, MD 20910, USA

Correspondence: Joost Buitink (joost.buitink@deltares.nl) and Brendan Dalmijn (brendan.dalmijn@deltares.nl)

This information product has been peer reviewed and approved for publication as a preprint by the U.S. Geological Survey.

Abstract. Climate change is expected to impact hydrological regimes worldwide, including the Pacific Northwest of the United States. This study investigates how climate change will affect river discharge in the Puget Sound region of the State of Washington, with a focus on King and Pierce Counties. We simulated river discharge under historical and future conditions using the physically based, spatially distributed wflow_sbm hydrological model, which was calibrated and validated against U.S. Geological Survey discharge records. Future forcing was based on an ensemble of six high-resolution CMIP6 climate models, which were bias corrected using empirical quantile mapping. The results indicate a decrease in summer discharges (5–10%) and an increase in winter discharges (5–10%) across the study region. The high discharges (90$^{\text{th}}$ percentile) are projected to increase in winter, and the low discharges are projected to decrease in summer, due to shifts in precipitation regimes, snowpack hydrology, and evapotranspiration. However, variability between individual CMIP6 models often exceeds the magnitude of ensemble mean changes, underscoring substantial uncertainty in climate projections and the importance of including multiple climate models in climate change analysis. Furthermore, model consensus increased with elevation, which could be the result of the higher elevation areas being driven by less diverse hydrological processes. These findings highlight potential challenges for regional water management, ecosystem health, and flood risk mitigation in the Puget Sound region under future climate conditions.

1 Introduction

Changing atmospheric and ocean temperatures are leading to pronounced changes in meteorological patterns and sea level rise around the world (Martel et al., 2021; Oh et al., 2024). These changes affect tides, storm surge, sea level anomalies, watershed runoff, sediments, and groundwater individually and cumulatively affect flood severity in complex ways (Grossman et al., 2023b; Nederhoff et al., 2024; Wahl et al., 2015). An estimated 600 million people in 2020 (and more than 1 billion by 2050) are expected to be exposed to flood hazards that affect human safety, economics, food security, and well-being (Edmonds et al., 2020; Merkens et al., 2016). Until recently, predictive models used to evaluate exposure and risk have emphasized single flood drivers or short-duration hydrological events (Fowler et al., 2021). With sea level rise and climate change driving changes in flood patterns across large spatial scales, the need for computationally efficient approaches to assess regional impacts and capture decadal climate variability has increased in importance.

Among the hydrological impacts of climate change, changes in magnitude, timing, and type of precipitation, as well as changes in glacier dynamics and interactions between groundwater and surface water, are altering hydrological conditions globally (Maity and Maity, 2022; Fowler et al., 2021; Abbass et al., 2022; Kotz et al., 2024). In the Pacific Northwest, these global climate-driven changes are projected to manifest themselves in distinct regional patterns. The precipitation is expected to intensify, to shift to more rainfall and less snowfall, and to have earlier rainfall in autumn, without changing the total annual precipitation. These changes in precipitation are likely to become more pronounced towards the end of the 21st century and are expected to substantially increase peak discharges (Mauger et al., 2015). Concurrently, drier summertime conditions will lead to smaller summer discharge and a reduced contribution of glacier melt (Yan et al., 2021). Similar to other coastal settings around the world, these changes in hydrology are expected to have pronounced effects on water supply and quality for urban purposes, agriculture, and ecosystem health, especially for temperature-sensitive fish and wildlife (Mauger et al., 2015).

Densely populated regions adjacent to major rivers and the coastline are likely to face the greatest consequences from climate-driven changes in hydrology, given their high concentration of people, infrastructure, and economic activities. In the Pacific Northwest, King and Pierce Counties encompass the most densely populated urban areas, including the Seattle-Tacoma metropolitan region, making them particularly vulnerable to changes in flood hazards and water resources. Changes in exposure to flooding across King and Pierce Counties in western Washington have already been documented with shifts in discharge due to the expansion of impervious surfaces associated with urban development (Moscrip and Montgomery, 1997; Cuo et al., 2009) and the rerouting and channelization of river discharge causing sedimentation and restricted drainage (Rosburg et al., 2017; Grossman et al., 2020). The projected increases in peak river discharge (Mauger et al., 2015) are expected to raise flood risk. At the same time, the shift toward autumn and winter discharges is expected to have complex impacts on hydroelectric production in this highly urbanized region. The compounding effects of an estimated 0.25–0.50 m of sea level rise (Miller et al., 2018; Grossman et al., 2022, 2023a) further threaten lowland areas where some of the region's highest population density and critical infrastructure are located.

Given these projected changes in hydrology and the potential for significant impacts, it is crucial to understand how river discharge and other hydrological responses may evolve under future climate conditions. During the previous decades, researchers have employed both statistical (Salathé Jr et al., 2007; Hamlet et al., 2013) and dynamic (Salathé Jr et al., 2014) approaches to assess changes in the hydrological response. Many of these studies have relied on hydrological models such as the Variable Infiltration Capacity (VIC, Liang et al., 1994) or the Distributed Hydrological Soil Vegetation Model (DHSVM, Wigmosta et al., 1994). Coupling these models with climate projections from the Coupled Model Intercomparison Project 3 (CMIP3, Salathé Jr et al., 2014) and CMIP5 (Mass et al., 2022), resulted in consistent findings for the Pacific Northwest, where peak discharges in winter are likely to increase and low discharges during summer are likely to decrease.

In this study, we combined the latest generation of climate projections from the Coupled Model Intercomparison Project Phase 6 (CMIP6) with a computationally efficient distributed hydrological model, to explore how recent advances in climate and hydrological models influence projections of the future hydrological response under climate change. We employed a high-resolution subset of the CMIP6 models (the High-Resolution Model Intercomparison Project, Haarsma et al., 2016; Nguyen et al., 2024), to ensure more realistic weather patterns simulated by the climate models. Our study focuses on the catchments located in King and Pierce Counties in the State of Washington which encompass the most densely populated areas of the Pacific Northwest. This makes them a critical case study for understanding hydrological responses, where climate-driven changes could have the greatest impacts on people, infrastructure, and regional water resources. In addition to analyzing the hydrological response driven by an ensemble of six CMIP6 models, we also examined the variability among individual models to assess uncertainty and inter-model differences in future river discharge projections.

2 Methods and data

2.1 Study area

This study focuses on the watersheds and river systems in King and Pierce Counties, Washington, that drain the western Cascade Range across the Puget Sound lowland to the eastern shore of the Puget Sound estuary (Fig. 1). King and Pierce Counties encompass areas of $\sim$ 5,700 km^2 and $\sim$ 4,400 km^2, respectively, and the simulated watersheds in King and Pierce Counties encompass an area of $\sim$ 3,000 km^2 and $\sim$ 5,000 km^2, respectively. From a hydrological perspective, terrain, climate, and urban development differ significantly between these two regions. The lowlands include areas of intensive agricultural use and high developed areas with urban infrastructure and stabilized river channels. Along the shoreline of Puget Sound, the Seattle-Tacoma metropolitan area represents the largest population center in the state, with 4 million inhabitants (more than half of the total population of the state, U.S. Census Bureau). The western parts of the King and Pierce Counties are sparsely inhabited and largely undeveloped. The transition to the Cascade Range also brings mountainous terrain, small high-gradient headwaters, glaciers, and seasonal snow pack.

This region has a temperate marine climate with warm, dry summers and cool, wet winters. The average annual precipitation in the Counties is about 2000 mm, ranging from about 1000 mm near Puget Sound (Tacoma) to more than 3800 mm in parts of the Cascade Range. The distribution of precipitation varies greatly seasonally with dry summers (mean total precipitation of 75 mm at Tacoma) and wet winters (mean total precipitation of 400 mm at Tacoma) (National Oceanic and Atmospheric Administration, 2020). Annual evapotranspiration is estimated to range from 380 to 600 mm (Richardson et al., 1968). Seasonal runoff is generally characterized by several high-flow periods in winter, medium discharges in spring, and sustained low river discharges in summer and autumn. Local geology is highly variable; however, the Puget Sound Lowland is generally composed of unconsolidated sedimentary deposits left by continental glaciers of the Pleistocene Epoch (Porter and Swanson, 1998; Collins and Montgomery, 2011), which transitions to Tertiary bedrock in the Cascade Range.

For King County, most river discharge is concentrated in three major basins: the Green-Duwamish, Lake Washington, and Snoqualmie Basins. The average annual runoff during the period 1931-60 for the Snoqualmie River Basin (1800 km^2) was approximately 2000 mm. During the same period, annual runoff in the Lake Washington Basin (1500 km^2) averaged about 800 mm, and in the Green-Duwamish River Basin (1250 km^2), about 1150 mm (Richardson et al., 1968). A substantial part of the overall drainage for King County has been dammed. In particular, the completion of the Howard Hanson Dam in 1962

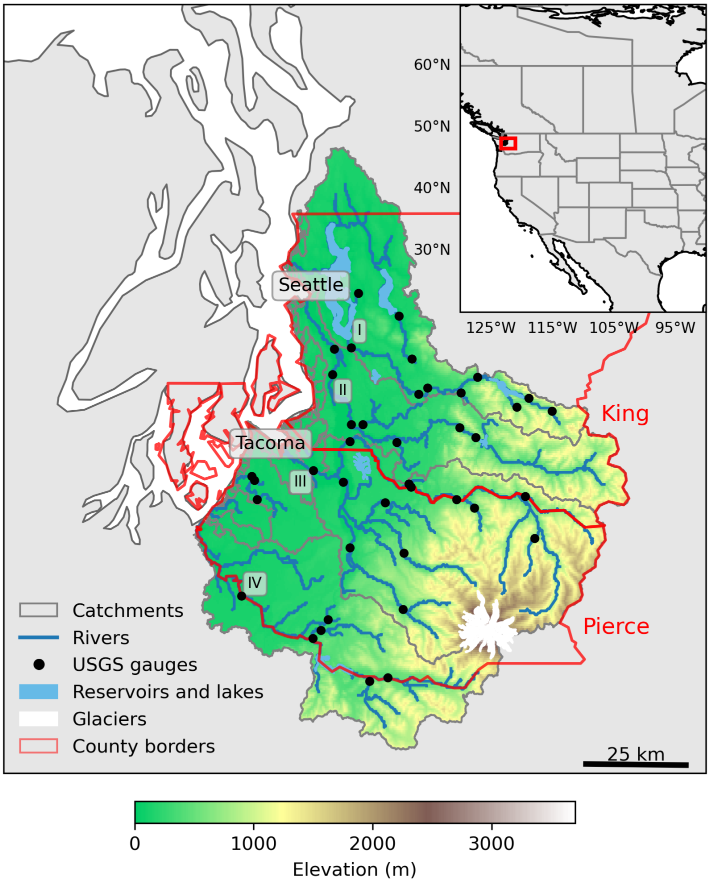

Figure 1. Spatial extent of the wflow_sbm models used in this study. Inset positions the extent of the main panel in North America. Note that the river and catchment delineations are plotted at the wflow_sbm spatial resolution of 500×500 meters. The borders of King and Pierce Counties are outlined in red. Four streamgages (U.S. Geological Survey, 2024) are labeled (I-IV), which are the four streamgages used in Tab. 2.

significantly changed the watershed dynamics in the Green-Duwamish River Basin. King County does not contain any glaciers, but seasonal snow processes strongly contribute to downstream hydrology.

Pierce County is composed of the White; Puyallup; Nisqually River, and the Key Peninsula and Gig Harbor. The Key Peninsula and Gig Harbor is physically disparate from the other watersheds (located on the west side of Puget Sound), and resides entirely in the Puget Sound lowlands, where river discharge is fully driven by precipitation. The White/Puyallup and Nisqually Rivers drain the partially glaciated Cascade Range and Mount Rainier. Similar to the Duwamish, the White/Puyallup watershed ends in a major urbanized zone (the city of Tacoma), where it has been substantially channelized and straightened from its natural course. The Nisqually watershed ends in a large, less developed river delta and is regulated by the Alder and La Grande Dams.

2.2 Data

2.2.1 Landscape data

The primary input datasets for any hydrological model are meteorological forcing fields and landscape data that define topography and soil/terrain characteristics. The land surface elevation and topography data were obtained from the National Elevation Dataset (Gesch et al., 2002). Soil properties were derived from SoilGrids (Hengl et al., 2017), and related soil parameters were estimated using pedo-transfer functions as described by Imhoff et al. (2020). Land cover properties and related parameters were derived from GlobCover 2009 (Arino et al., 2009). MCD15A3H Version-6 leaf area index product (Myneni et al., 2015) was used to derive Leaf Area Index (LAI) climatology. The Randolph Glacier Inventory 6.0 (Pfeffer et al., 2014) provided information on glacier locations. The dataset from Lin et al. (2020) was used to extract river widths and to derive the river depth values based on the bankfull discharge provided in the dataset. The Global Reservoir and Dam Database (GRanD, Version 1, Revision 01 (v1.01), Lehner et al., 2011) and HydroLAKES (Version 1.0, Messager et al., 2016) were utilized to identify reservoir and lake locations and to derive the required parameters and characteristics, such as area and depth.

2.2.2 Meteorological data

In this study, two sources of meteorological data were used: a reanalysis dataset for the calibration of the hydrological model and the CMIP6 climate model dataset (Eyring et al., 2016, which was bias-corrected using on the reanalysis dataset). For this paper, ERA5 was selected to provide the reanalysis meteorological data (Hersbach et al., 2023). ERA5 offers a variety of advantages over other meteorological datasets, including a globally consistent extent, all necessary data variables for wflow_sbm, a long record length (1940 to the present), and a temporal resolution of 1 hour. ERA5 is a fully data-assimilated reanalysis product, which means that modeled meteorological data are combined with data from observations to improve modeled output. The variables used from ERA5 for this analysis included: precipitation, temperature (at 2 meters), radiation (short-wave incoming) and pressure (at mean sea level).

An additional reason for selecting the ERA5 dataset is that the model spatial resolution of ERA5 is similar to that of the CMIP6 models. Input data spatial resolution is an important factor in hydrological modeling, so ideally the model is calibrated and validated with a similar input field spatial resolution. Validating the model on higher spatial resolution data would provide an unrealistic view of the model performance when utilizing a coarser spatial resolution meteorological forcing. Therefore, ERA5 was selected, even though higher spatial resolution data were available for some input variable fields (e.g., precipitation).

2.2.3 Discharge data

Observed discharge data were used in the study for model calibration and validation (40 U.S. Geological Survey streamgages, refer to black circles in Fig. 1). Discharge observations for all available streamgages within the Counties were downloaded directly from the U.S. Geological Survey National Water Information System (NWIS; U.S. Geological Survey, 2024), and we downloaded all available data between 1987 and 2023 (with varying coverage per location). Discharge data were available at a temporal resolution of 15 minutes but were resampled (mean) to a temporal resolution of 3 hours to match the inputs from the CMIP6 model and the simulation output.

2.2.4 Climate data

Our best understanding of how the climate is changing over large time scales is provided by global climate models (GCM's). GCM's simulate the entire Earth system to determine how changes to greenhouse gas emissions and other forcings broadly affect climate patterns. GCMs have been shown to reproduce global patterns well, but are susceptible to bias and errors at the regional to local scale (Haarsma et al., 2016) primarily because of the inability to resolve physical interactions at coarse spatial resolutions of 1 to 3 degrees longitude (at the equator 111 to 334 km). The Coupled Model Intercomparison Project 6th iteration (CMIP6, Eyring et al., 2016) provides the most recent projections of future global atmospheric change with a collection of over 100 global climate models and experiments.

As mentioned above, most CMIP6 models in this collection have coarse spatial resolution (typically 1^{o} or larger). Because the area of interest for the paper can be considered 'local' (a few degrees longitude and latitude) and hydrology is strongly influenced by input field resolution, this study used a high-resolution subset of the CMIP6 models: the High-Resolution Model Intercomparison Project (HighResMIP; Haarsma et al., 2016; Nguyen et al., 2024). The HighResMIP project only features a few of the models in the CMIP6 collection and has a shorter temporal length (1950–2050), as compared to the standard CMIP6 models which were run to 2100. The climate models utilized for this study are based on the Shared Socioeconomic Pathway 5-8.5 (SSP5-8.5, similar to the RCP8.5 scenario).

To limit biases among individual CMIP6 models and to improve the robustness of the resulting climate change signals, it is best practice to consider an ensemble of CMIP6 models (Nouri and Veysi, 2024). This study utilized an ensemble of six GCMs, each containing the same variables as those used in ERA5. Although most of the variables in the climate models were available at a temporal resolution of three hours, this was not the case for all variables (refer to Table 1). A temporal resolution coarser than 6 hours was deemed too coarse because peak discharges occur at the scale of a couple of hours and using inputs coarser than 6 hours would cause an under-prediction of peak river discharges due to averaging across peaks. The chosen 6 CMIP6 models feature a 3-hour output resolution for most of the necessary variables (refer to Table 1), which is the highest available temporal resolution. As a result, a temporal resolution of 3 hours was chosen for the simulations.

Table 1. Variables used in this study and their temporal frequency (in hours) for each of the HighResMIP models. Precipitation (Precip.) is total precipitation (snow and rain) in kg m^{-2} s^{-1}. Temperature (Temp.) is measured at 2 meters above the terrain and is in degrees Celsius. Radiation (Rad.) stands for short-wave incoming radiation (W m^{-2}). The pressure (Press.) is measured in mean sea level (MSL) in Pascals.

CMIP6 model	Variant	Precip.	Temp.	Rad.	Press.	Spatial resolution
CNRM-CM6-1-HR	r1i1p1f2-gr	3	3	24	6	0.5° x 0.5°
EC-Earth3P-HR	r1i1p1f1-gr	3	3	24	6	0.35° x 0.35°
GFDL-CM4C192-highresSST	r1i1p1f1-gr3	3	3	24	6	0.625° x 0.5°
HadGEM-GC31-HH-highres	r1i1p1f1-gn	3	3	24	3	0.35° x 0.23°
HadGEM3-GC31-HM-highres	r1i1p1f1	3	3	3	3	0.35° x 0.23°
HadGEM3-GC31-HM-highresSST	r1i1p1f1-gn	3	3	24	3	0.35° x 0.23°

Model variables with native temporal resolution coarser than the 3-hour time-step were either resampled directly (in the case of 6-hour temporal resolution), i.e. values from the coarser temporal resolution data were copied, or resampled using a daily pattern (in the case of 24-hour temporal resolution). The daily pattern was derived from the ERA5 daily pattern. For this purpose, ERA5 was resampled to match the spatial resolution of the specific climate model.

2.3 Hydrological modeling

2.3.1 The wflow_sbm model

To simulate all relevant hydrological processes, the wflow_sbm model hydrological model was used (Van Verseveld et al., 2024). This is a physically based, spatially distributed hydrological model. The wflow_sbm model was built on the vertical SBM concept (simple bucket model, based on the Togo_SBM concept from Vertessy and Elsenbeer, 1999), and uses a kinematic wave assumption for subsurface and overland flow, and the local inertial approximation for river discharges (including a 1-D floodplain schematization). A conceptual overview of the wflow_sbm model is presented in Fig. 2. More information, details and equations can be found in Van Verseveld et al. (2024).

We built two separate wflow_sbm models, one for each county. Each model contains several different subbasins, as shown in Fig. 1. These models were built using the Python library HydroMT-wflow (Eilander et al., 2024), which is based on HydroMT (Eilander et al., 2023).

The models were built with a spatial resolution of 500 $\times$ 500 meters, and were run on a 3-hour time interval. This spatial resolution was selected as an optimal balance between spatial heterogeneity, computational requirements, and the optimal range identified in Aerts et al. (2022). Moving to 500 $\times$ 500 meters instead of a finer resolution of e.g. 250 $\times$ 250 meters cuts the calculation time in half while sacrificing minimal spatial information at the scale of the catchments in King and Pierce Counties.

Van Verseveld et al. (2024) shows six case studies in which wflow_sbm has been applied to different regions of the globe and different catchment scales. The six case studies demonstrated good model performance compared to discharge observations,

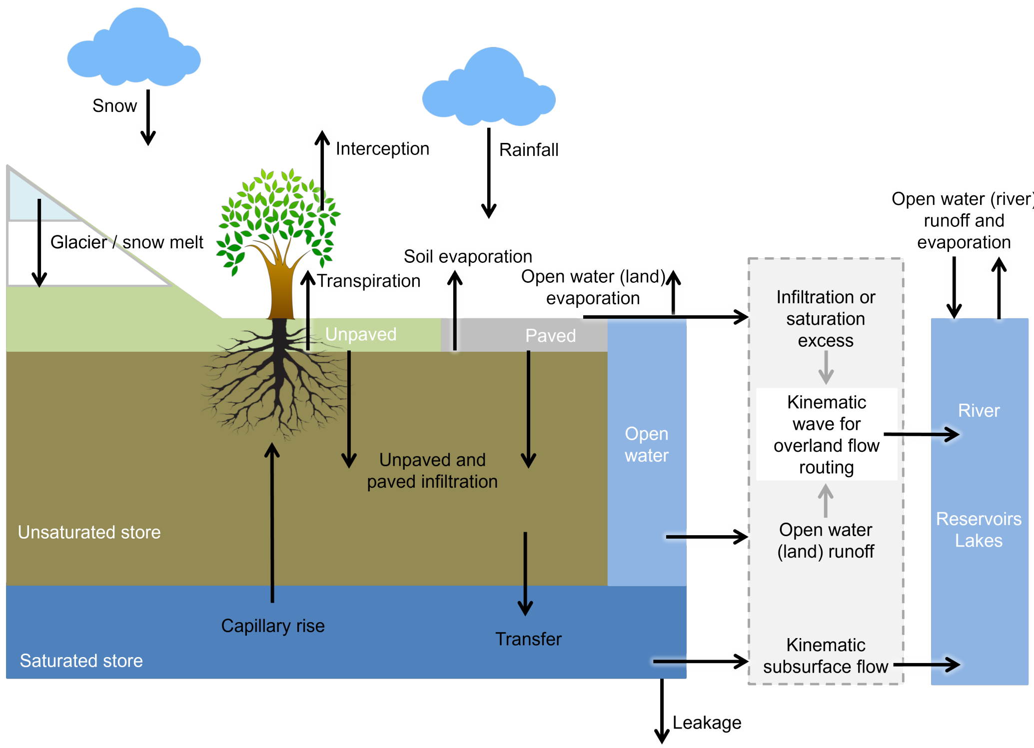

Figure 2. Conceptual overview of the wflow_sbm model, figure adapted from Van Verseveld et al. (2024).

often with little or no calibration due to parameter estimation as described by Imhoff et al. (2020). Furthermore, the wflow_sbm model was used to calculate inflow timeseries for more than 3,000 reservoirs globally (van der Laan et al., 2024), where the authors reported good agreement with measured/derived reservoir storages, indicating that the model was able to properly capture the hydrological processes across different continents. Aerts et al. (2022) applied the model to a large sample of basins in the CAMELS dataset, demonstrating relatively good performance over the US, especially in the north-west and along the east coast. Furthermore, Imhoff et al. (2024) applied the model to cover Europe and achieved King-Gupta efficiency (KGE) values of at least 0.5 for more than 55% of the Global Runoff Data Centre stations, without any calibration. Locations with poorer model performance were mostly very small tributaries.

2.3.2 Calibration procedure

Calibration of hydrological models is commonly done by comparing the modeled discharge with the discharge obtained from observation stations (streamgages) to determine which combination of parameter values yields the best performance. From the wflow hydrological model, three parameters were selected for calibration: *KsatHorFrac* (defined as the ratio between saturated horizontal and vertical conductivity), rooting depth, and soil thickness. These parameters each influence different hydrological processes and contribute to the overall 'responsiveness' of the model, i.e., essentially how long it takes for water to reach the rivers.

Prior to calibration, we ensured accurate reservoir behavior by manually modifying the reservoir parameters in the wflow_sbm models. Initial estimates were provided by the HydroMT-wflow model builder based on the GRanD and HydroLAKES datasets (refer to Sect. 2.2.1). After this initial estimate, we used historical timeseries available from ResOpsUS (Steyaert et al., 2022) to further fine-tune the reservoir parameters (average outflow, spillway capacity, and target full and empty fractions). If no data were available from the ResOpsUS dataset, we used downstream discharge observations to improve the parameters.

Sufficient observation stations (40 stations, refer to black circles in Fig. 1) were available within King and Pierce Counties to calibrate at a subbasin level. As a result, the wflow models were calibrated utilizing a cascading methodology, where we progressed from the upstream subbasins to the downstream subbasins. All subbasins are categorized into four levels, where each level corresponds with the number of subbasins upstream of the subbasins in that level. Subbasins in level 1 have no upstream subbasins, subbasins in level 2 have one upstream subbasin, subbasins in level 3 have two upstream subbasins, and subbasins in level 4 have three upstream subbasins.

After the calibration of each level, the best-performing parameter set was chosen for all subbasins within that level. These parameters were then used in the calibration of the next level to ensure that subsequent calibrations were built on the best performing parameters from the previous level. After the last level of calibration, the entire model is considered calibrated.

As mentioned above, the best performing parameter set is obtained by comparing the modeled discharge with the observed discharge. This comparison is summarized into a single metric that represents the 'goodness' of the fit. For this case, three metrics were chosen to equally focus on the general behavior of the model and the larger/more extreme discharge events. To evaluate the general behavior of the model, the Kling-Gupta efficiency (KGE) coefficient (Gupta et al., 2009) was chosen, which is defined as follows:

$$\varepsilon = 1 - \sqrt{(r-1)^2 + (a-1)^2 + (b-1)^2} \tag{1a}$$

where

$$r = \frac{\sum_{i=1}^{n}(o_i - \mu_o)(s_i - \mu_s)}{\sqrt{\sum_{i=1}^{n}(o_i - \mu_o)^2}\sqrt{\sum_{i=1}^{n}(s_i - \mu_s)^2}}, \;\; a = \frac{\sigma_s}{\sigma_o}, \;\; b = \frac{\mu_s}{\mu_o} \tag{1b}$$

where s denotes the simulated discharge, and o the observed discharge, σ represents the standard deviation, and μ the mean.

For the evaluation of the larger discharge events, a combination of two metrics was chosen. First, the rising limb density was used (Shamir et al., 2005) to evaluate the response time of the system (i.e., its flashiness). The rising limb density essentially is a way of measuring the time it generally takes for the hydrograph to rise during significant discharge events. It is defined as follows:

$$\varepsilon = 1 - \left|1 - \frac{rl_s}{rl_o}\right| \tag{2a}$$

where

$$rl = \frac{n}{\sum_{i=1}^{n} T_i} \tag{2b}$$

where T represents the time the hydrograph rises during an event.

Second, the peak distribution (Euser et al., 2013) was used to evaluate whether the magnitudes of the peak discharges (i.e., local maxima) are similar between observed and modeled data. This evaluation is performed by examining the slope of the flow duration curve between two quantiles. The chosen quantiles were the 90th and 50th quantile. These two quantiles ensure that only the larger local maxima representing significant discharge events but not extremes are included because these are often the most hydrologically relevant (Euser et al., 2013; Sawicz et al., 2011). The peak distribution is defined as follows:

$$\varepsilon = 1 - \left|1 - \frac{p_s}{p_o}\right| \tag{3a}$$

where

$$p = \frac{q_{90} - q_{50}}{0.9 - 0.5} \tag{3b}$$

where q_x represents the discharge value corresponding to the 90th and 50th quantile.

The chosen metrics were combined into a single number for evaluation using a weighted Euclidean distance. When looking at the individual metrics, all metrics are set up in such a way that a value closer to one indicates better model performance. In contrast, for the Euclidean distance, a value closer to zero indicates better overall performance.

$$r = \sqrt{\sum_{i}^{n} w_i (1 - \varepsilon_i)} \tag{4}$$

The Rising Limb Density and the Peak Distribution heavily focus on the flashiness (i.e., high discharge events) of the hydrograph. Therefore, assigning a combined weight greater than 0.5 to these metrics would place insufficient emphasis on the general behavior of the hydrograph. To balance the focus between overall model behavior and high discharge events, the KGE coefficient alone was assigned 50% of the total weight. The remaining 50% was divided equally between the Rising Limb Density and Peak Distribution metrics.

The calibration period was selected as calendar year 2012–2018 during which sufficient data were available. Given that these were also recent years, we ensured that the model was able to accurately capture the recent historical response of the system. To ensure that the initial conditions of the hydrological model did not affect the performance, simulations were initialized in 2010, and the first two years were treated as a spin-up period and discarded for the metric calculations. The years 2019—2022 were used for model validation because these years also contained sufficient discharge observations.

2.4 Climate scenarios

2.4.1 Bias correction

The CMIP6 models provided the forcing climate data for the hydrological model for both the historical period and the future period. However, global climate models can contain biases on a regional scale (Sorland et al., 2018), so the selected CMIP6 models were evaluated for biases through a comparison with ERA5 reanalysis data. ERA5 was selected as the reference dataset for bias correction because observational data were not available at the spatial and temporal scales necessary for this study. In the area of interest (King and Pierce Counties), the CMIP6 models generally showed lower values of precipitation and higher values of temperature compared to ERA5. Because these variables (especially precipitation) have a high impact on the modeled discharge, it was deemed necessary to correct the CMIP6 model timeseries for these biases.

The empirical quantile mapping (EQM) method was selected for bias correction. This method has been shown to be a reasonable choice for bias-correcting climate model timeseries (Lehner et al., 2021). The bias correction was performed at the pixel level. The EQM method assumes that the quantiles of a dataset/signal (i.e. the shape of the cumulative distribution function [CDF]) are correct when compared to a reference signal that represents the actual situation. However, the EQM method states that the absolute values corresponding to the quantiles differ from the reference dataset (Fig. 3). Therefore, adjustment factors are determined based on discrete intervals of quantiles, where each interval gets one adjustment factor to adjust the values that correspond in that interval (e.g., one adjustment factor for an interval from 0.5 quantile to 0.75 quantile). The discrete quantile intervals were equally spaced from the 0.01 quantile to the 0.99 quantile with widths of approximately 0.0333. Beyond the 0.01 and 0.99 quantiles, the adjustment factors were extrapolated.

An example of quantile mapping is displayed in Fig. 3, where the temperature at a specific quantile (0.9), is shown before and after quantile mapping. A comparison of the temperature values of EC-Earth specifically (Fig. 3b) with the values of ERA5 (Fig. 3a) shows that EC-Earth generally overestimates the temperature in the 0.9 quantile. Examining the CDF curves (Fig. 3d) of EC-Earth's and ERA5's temperature, taken at roughly the location of Tacoma, Washington, reveals an overestimation of the temperature in the higher quantiles (and therefore the 0.9 quantile). After adjustment of the values based on the adjustment factors per interval, the values more closely match ERA5 (Fig. 3c).

2.4.2 Simulation setup

After bias correction, the timeseries from the CMIP6 models were used as forcing conditions (i.e., precipitation, temperature and evaporation) for the wflow model. The period from 1970 until 2014 was chosen as the 'historical' period of the simulation due to consistent coverage by all CMIP6 models. However, of these 45 years of data, only 35 years (1980–2014) of were used to match the length of the data of the future period (below).

The future period from 2015 to 2050 was chosen because the high resolution CMIP6 models only provided data until 2050. This horizon is similar to the 'near' future in accordance with the Intergovernmental Panel on Climate Change (IPCC), which defines the 'near' future horizon as the period from 2020 until 2040. The model states, such as the state of the glaciers at the end of the historical period, were used as initial states for the future horizon to negate the need for a warm-up period.

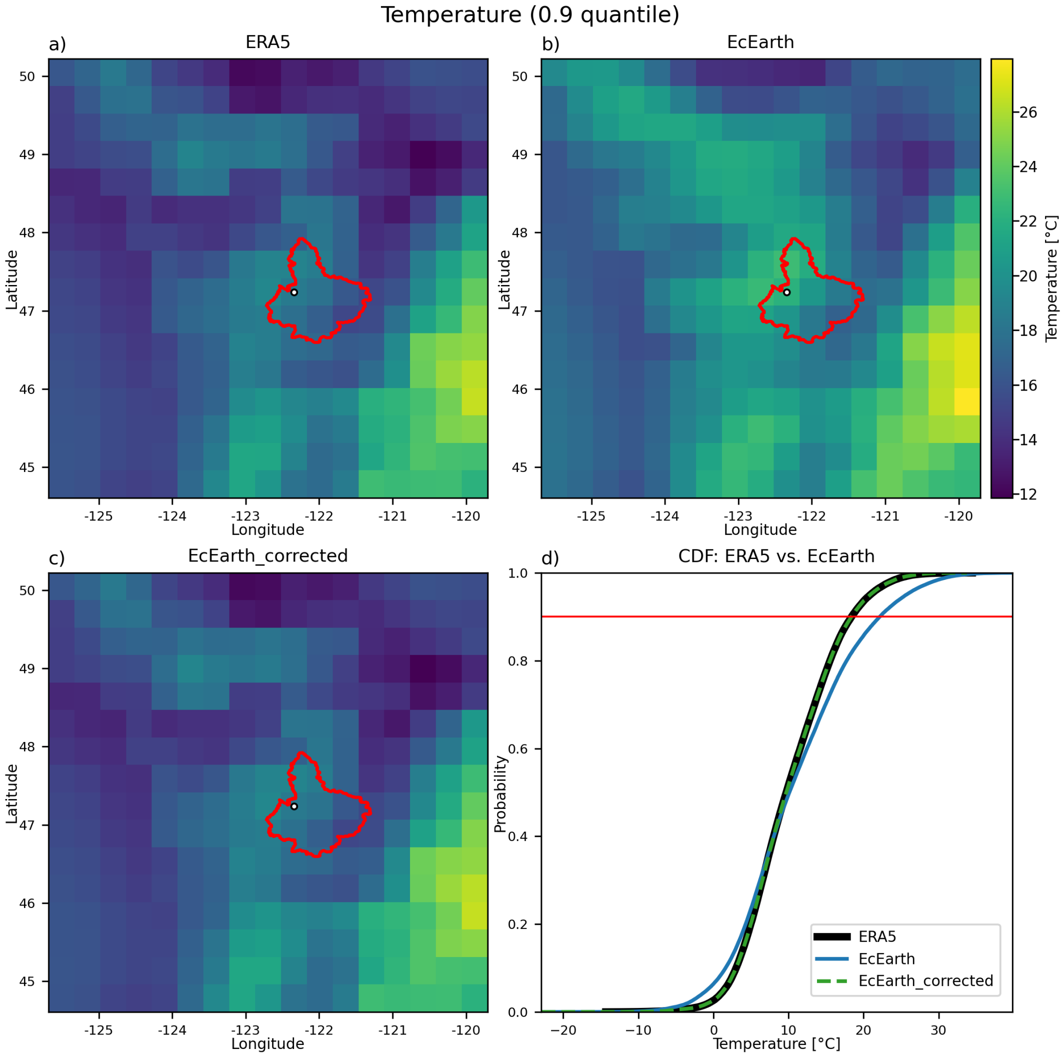

Figure 3. The impact of the bias correction on the temperature of the EC-Earth climate model. In the spatial figures (a, b and c), the outline of the basins within King and Pierce Counties are highlighted in red. In (a), the ERA5 temperature at the 0.9 quantile is shown. In (b), the uncorrected temperature of EC-Earth at the 0.9 quantile is shown. In (c), the bias corrected temperature at the 0.9 quantile is shown. In (d), the CDF curves at 47.239^{o} latitude and -122.344^{o} longitude (Tacoma, the white dot in a-c) are shown for ERA5, EC-Earth and the corrected EC-Earth. The red line in (d) is the 0.9 quantile.

2.4.3 Calculating changes

To allow a fair comparison of the climate signal projected by the different CMIP6 models, we calculated the relative change in the four hydrological metrics (average, 7-day minimum, 90th percentile and maximum discharge). In this paper, we chose to present only the 90th percentile discharge results because these provide a slightly more robust indicator for high discharge conditions. The results based on maximum discharge are included in the appendix. For the 7-day minimum discharge, we retained the minimum values because these already incorporate a rolling window of 7 days before computing the minimum value. These hydrological metrics were aggregated into three temporal periods: annual, summer half-year (April–September), and winter half-year (October–March). The metrics were calculated at the locations of USGS streamgages (Fig. 1) to ensure that the results are provided at recognizable and relevant locations.

To calculate the relative change per metric and aggregation period, the same number of years (35) was selected from the future period (2015–2050) and the historical period (1980–2015). To express these as relative changes, both historical and future values were sorted in ascending order, and a piecewise relative comparison was performed. This resulted in 35 relative changes, representing the relative change over the full range of data.

We combined the relative changes of all six CMIP6 models to describe the "ensemble" change, where the ensemble refers to the different CMIP6 models. To compare the response of individual climate models with the response of the ensemble of six models, the mean relative change was calculated for each climate model and the ensemble. The sign of the mean relative change was used to classify the direction of change. To determine the robustness of this change, we tested whether the standard deviation of the underlying relative changes was larger than the mean relative change based on the reasoning that when the variability of the data is smaller than the mean change, one can be reasonably confident in the direction of change and vice versa.

3 Results

3.1 Model performance for calibration and validation periods

The result after the calibration procedure is shown in Fig. 4 for a single observation point (Puyallup River, Pierce County). This figure shows substantial improvements to the simulated discharge after calibration. In particular, both the peaks and recessions are captured more closely in relation to observations after calibration as a result of a better 'tuning' of the parameters that influence the responsiveness of the system (model). These patterns are especially visible in the hydrograph for 2016 (Fig. 4d).

Figure 5 gives a spatial overview of the performance of the wflow_sbm discharge for all USGS streamgages in the study region. The figure shows that, for most streamgages, KGE values > 0.6 are achieved (n=27 of 40), both in the calibration and validation periods. Seven streamgages show KGE values < 0.4, but these are mostly streamgages within small watersheds (i.e. average discharges less than 1,000 $m^3 s^{-1}$). The streamgages at the outlet of large basins generally show very good model performance (KGE > 0.7). An outlier in this regard is the USGS streamgage 12089500 (located along the Nisqually River in the southwestern corner of the study area), despite showing better model performance for the upstream streamgages. It should be

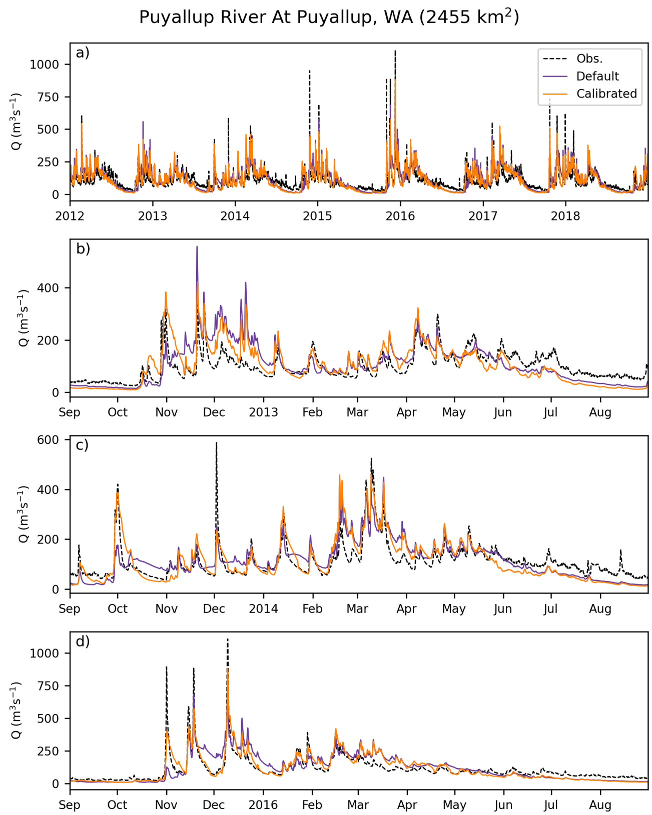

Figure 4. Discharge (Q, in cubic meters per second) timeseries for the calibration period (panel a) showing the difference between the simulated (purple and orange lines) and observed values (dashed black line), shown for USGS station 12101500 (refer to streamgage "III" in Fig. 1). The drainage area upstream of the streamgage is shown in parentheses. The bottom three panels are zoomed into the hydrological years 2013, 2014, and 2016 (panels b, c, and d, respectively). The label "Default" refers to the result of the uncalibrated model, and "Calibrated" as the result after the calibration procedure.

noted that the Centralia Canal diverts water from the Nisqually River for hydropower purposes. This diversion of water occurs upstream of USGS streamgage 12089500, and the divergence of a river is not supported by the wflow_sbm model. As a result, modeling the discharge accurately at this streamgage is difficult.

Additionally, model performance is relatively consistent between the calibration and validation periods (Table 2). Typically, models lose some performance when switching to a validation period because the model parameters are tuned for optimal performance for the calibration period. Only minor losses in performance (and even small increases for some streamgages) in the validation period gives confidence that the model is not overfit and therefore can robustly capture the hydrological response of this region. The values in Tab. 2 were taken from the most downstream streamgages of the larger rivers of King and Pierce Counties because these are most relevant from a hydrological and impact perspective. The lower KGE value observed at USGS

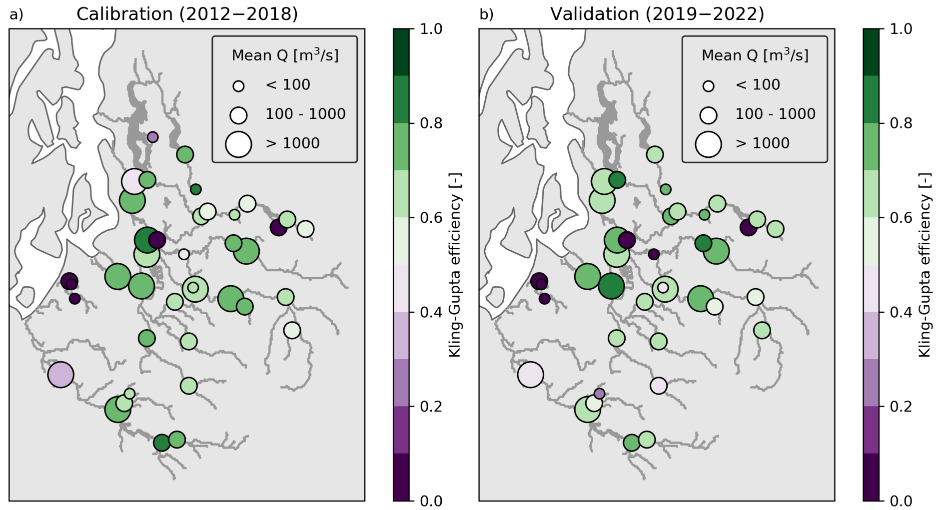

Figure 5. Model performance quantified using the King-Gupta efficiency (KGE) for the calibration (panel a) and validation (panel b) periods. Each dot represents an USGS observation station, the size indicates the average measured discharge (based on the available data between 1987–2023), and the color indicates the KGE value. Stations with less than 25% data coverage in the time period are discarded.

Table 2. Kling-Gupta efficiency values over the calibration period (2012-2018) and the validation period (2019-2022). The letter between brackets after the USGS gauge number (U.S. Geological Survey, 2024) links to the highlighted streamgages in Fig. 1.

River	USGS gauge	KGE (calibration)	KGE (validation)
Cedar River	12119000 (I)	0.76	0.82
Green River	12113344 (II)	0.76	0.63
Puyallup River	12101500 (III)	0.77	0.76
Nisqually River	12089500 (IV)	0.38	0.44

streamgage 12089500 is likely the result of an upstream diversion of water into a man-made canal that reconvenes downstream of the streamgage, which is not accounted for in the hydrological model, as mentioned before.

3.2 Effects of climate change

Figure 6 shows the effect of the changing climate on average discharge, and shows a consistent decrease in discharge across the entire study area. Average annual discharge is projected to drop by about 5%. Only one streamgage shows an increase (in the southeastern mountainous region), but this increase is minor (between 0–5%). The effects of climate change are more pronounced when exploring the changes for the winter and summer half-years.

In contrast to annual average changes, average winter discharge is expected to increase in most locations. Most increases are in the 5–10% range, but some locations show an increase of more than 10%. These locations are mostly smaller upstream

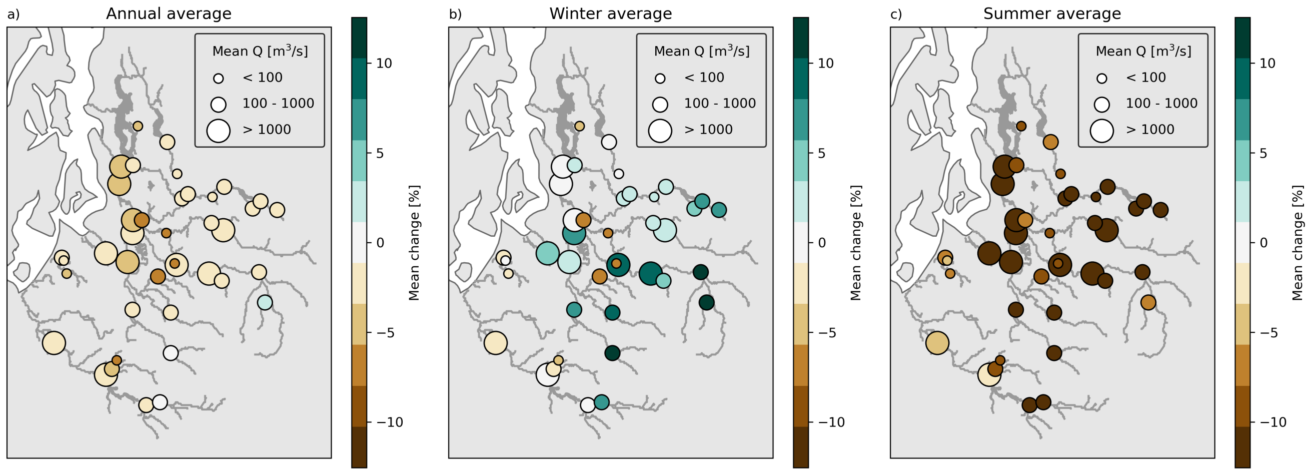

Figure 6. Change in average discharge for each USGS station, show for the annual, winter and summer periods (panels a, b, and c, respectively). The colored value represents the mean value of all relative changes from all considered CMIP6 models. The size of the dot indicates the average measured discharge.

basins (close to Mount Rainier). Increases in winter discharges indicate an increase in precipitation, a change from snowfall to liquid precipitation, or a combination of both. The average discharge during the summer period shows strong and consistent decreases throughout the entire area, with many locations projecting a reduction of more than 10% in average discharge. In addition, locations that show a relatively strong increase in winter discharge also show a strong decrease in summer discharge. These trends suggest that the seasons are roughly opposites, resulting in a small decrease in the amount of discharge when averaged over the full year.

Not only is the average discharge expected to change, but high discharge events are also expected to change under climate change scenarios (Fig. 7). Despite the expected decrease in the average annual discharge, the annual 90th percentile of discharge is projected to increase. However, this increase is not as pronounced as the change in average discharge, with most increases being in the 2–5% range. Furthermore, some locations also show a slight decrease of about 5–7.5%. Just like with average discharge, changes are more pronounced when grouping results into winter and summer half years. The 90th percentile discharge values show a much stronger increase in winter, while the summer period shows a uniform decrease across all locations. Most locations that showed little to no change for the annual values showed opposite change in the winter and summer changes, which almost fully compensated to only a minor difference on the annual temporal scale.

In contrast to the average and 90th percentile discharge values, the changes in the 7-day minimum values show the same signal for the annual, winter, and summer periods. Additionally, the changes for the 7-day minimum discharge are substantially larger: the changes in average 90th percentile discharge were all in the range of 10% (both increases and decreases) and the 7-day minimum values were projected to decrease by about 20–40%, depending on the location. The largest decreases were projected in summer, but even in winter there were decreases of about 10–20%. The decreases can largely be explained by an

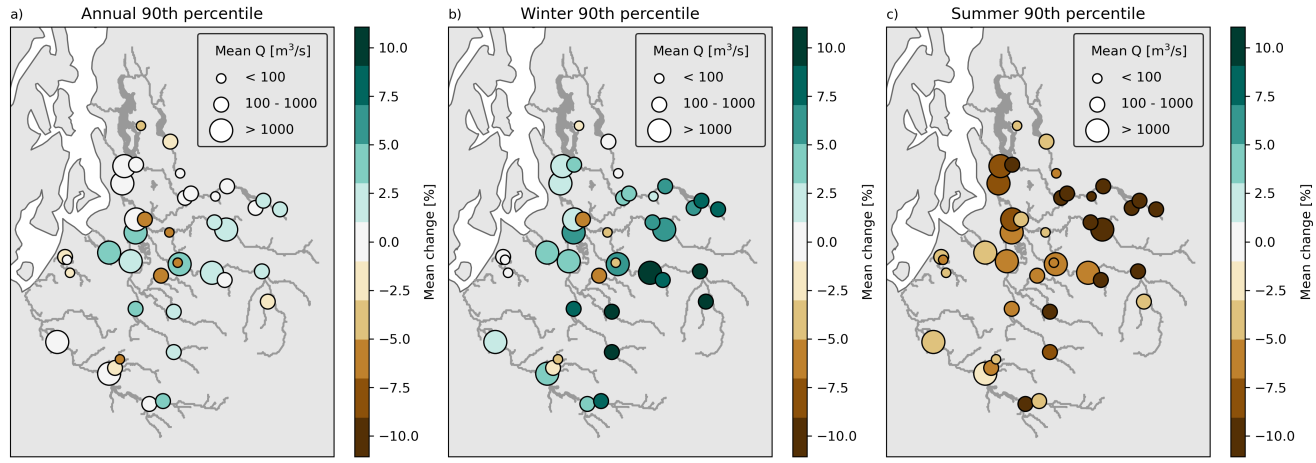

Figure 7. Change in 90th percentile discharge for each USGS station, show for the annual, winter and summer periods (panels a, b, and c, respectively). The colored value represents the mean value of all relative changes from all considered CMIP6 models. The size of the dot indicates the average measured discharge.

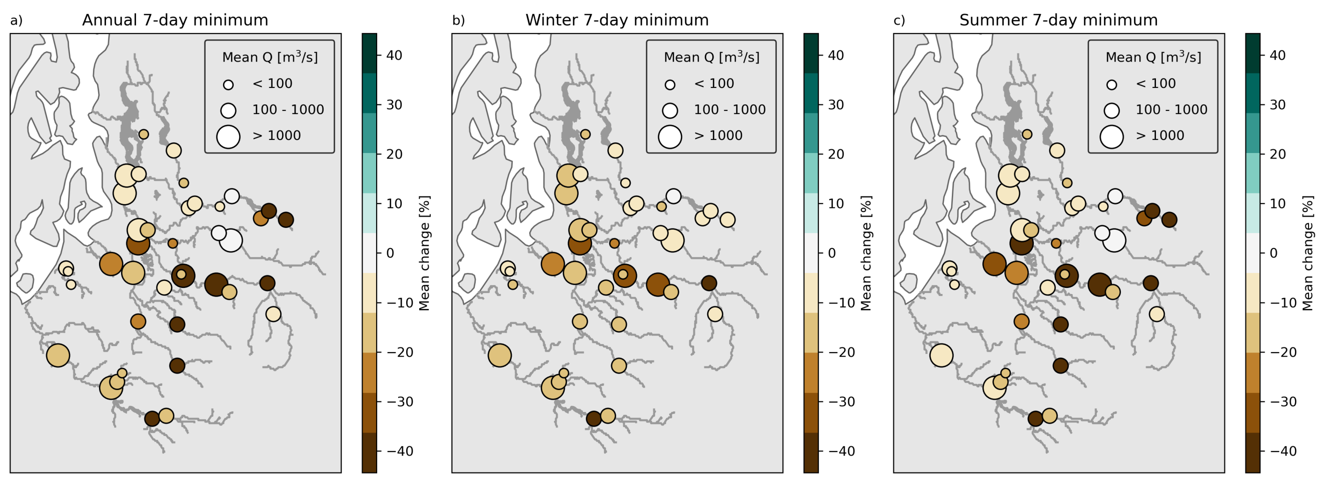

Figure 8. Change in 7-day minimum discharge for each USGS station, show for the annual, winter and summer periods (panels a, b, and c, respectively). The colored value represents the mean value of all relative changes from all considered CMIP6 models. The size of the dot indicates the average measured discharge.

increase in air temperature, leading to more evapotranspiration and less snowfall, and therefore a reduction in 7-day minimum discharge.

3.3 (Dis)agreement between climate models

The inclusion of six different CMIP6 models in this study allowed additional analysis of the response of each climate model and how it compared to the ensemble of all six models. The results for the average discharge, 90th percentile discharge, maximum discharge and 7-day minimum discharge can be found in Figs. 9–11, respectively. These figures show the sign of change as described by the full ensemble of six models and the sign of change as described by each individual climate model. For average discharge (Fig. 9), there are only clear signals in the ensemble change visible in the summer average discharge, all indicating a decrease in summer averages. For annual and winter averages, the full ensemble did not indicate a clear change, only an increase for three upstream locations for the winter average discharge. In general, locations showing a large relative change from the ensemble are also the locations that show a clear sign of change by the individual models. This indicates that locations that do not show a large relative change are likely to show a larger variability between the different climate models. This is visible in the panel showing the sign of change for the annual average (Fig. 9a), where zero locations show a clear signal based on the full ensemble, but individual climate models tend to show a sign of change. In contrast, the response in summer becomes much more uniform, where the full ensemble shows a clear decrease in average summer discharge for most locations, and the individual models tend to form a more uniform response, with most individual models also showing a decrease for most locations. It should be noted that for low flows, there are large similarities between the annual and summer panels because the annual low flows are dominated by the summer low flows. The same holds for the 90th percentile discharge, where the high flows typically occur in winter and therefore largely affect the annual values.

A similar response is visible for the results based on the 90th percentile discharge (Fig. 10). The annual values (Fig. 10a) show that the individual climate models tend to show a varying response: models indicating an increase, decrease, and no clear signal for multiple locations. As a result, the overall ensemble does not show a clear signal for any location. Only for the winter values (Fig. 10b), two locations are highlighted as showing an increase by the ensemble. The individual climate models runs tend to show fewer decreases and slightly more increases or no change, as indicated by the reduction of brown triangles in the pie charts. Similar to the average values, the summer values show a clearer signal of a decrease in 90th percentile discharge. Furthermore, the individual climate models show a more consistent pattern on decreases and only show an increase for one location. Despite this, only a limited number of locations are flagged as showing a clear decrease based on the ensemble of climate models.

Figure 11 shows a similar map, but for the 7-day minimum discharge. In contrast to the previous two discharge indicators, the ensemble shows a clear response for most locations on an annual level. Not a single climate model shows an increase for any location on the annual level. The pattern is similar to the summer values (Fig. 11c). Only winter contains a few locations with a single climate model that project an increase. Overall, the response for the 7-day minimum discharge is very consistent and more consistent than the high and average discharge metrics.

To explore the spread of the different climate models for all locations, we plotted the changes projected by the ensemble and the individual climate models against the elevation of the streamgage locations for the average and 90th percentile discharge

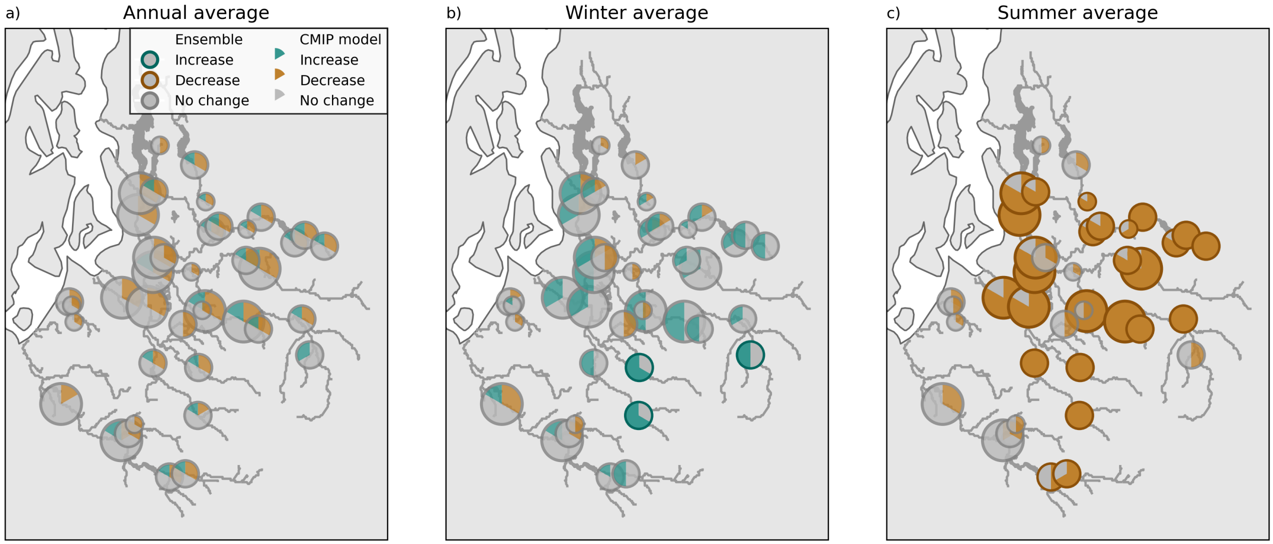

Figure 9. Sign of change in average discharge as predicted by the ensemble of climate models (outlines) and the individual CMIP models (pie chart) at USGS streamgage locations. The size of the circle is related to the average observed discharge (e.g., Fig. 5). The six CMIP models build up the pie chart and are sorted by their sign, so the exact location of each CMIP model can change per location/panel. Blue colors indicate an increase, brown colors indicate a decrease, and gray color indicate no clear change. If the ensemble data did not indicate a clear change, the circle and pie chart is made slightly transparent to improve emphasis on locations with a clear change.

(Figs. 12 and 13, respectively). As the pattern for the 7-day minimum discharge was so consistent, we decided to include these figures in the appendix (Fig. A4).

The relation between elevation and average discharge (Fig. 12) shows some interesting patterns. First, for the annual average discharge (panel a), values are fairly consistent across the full elevation range. The spread per location shows a slight decrease with elevation, where the lower-elevation streamgages ranged between -15% and +5% and the streamgages at higher elevations ranged between -7% and +8%. There appears to be a small positive trend with increasing elevation, but this trend is well within the spread between the different climate models. A trend with elevation becomes much clearer when looking at winter and summer values (Fig. 12b and Fig. 12c, respectively). The average winter discharge shows a clear positive trend with elevation, indicating a stronger increase in the average winter discharge for higher-elevation locations. In contrast, the average summer discharge shows a negative trend with elevation, indicating a stronger decrease in summer discharge for lower-elevation locations. These contrasting patterns in summer and winter are offset on an annual level. For these three panels, the response per climate model is also consistent: the positions/order of the individual climate models does not substantially vary with increasing elevation.

Figure 13 shows the relation between elevation and the 90th percentile discharge. Similar to the average discharge, with increasing elevation these results show: (1) a reduction in spread for the annual values, (2) a positive trend for the winter values, and (3) a negative trend of summer values. The slight positive trend observed for the annual average discharge is

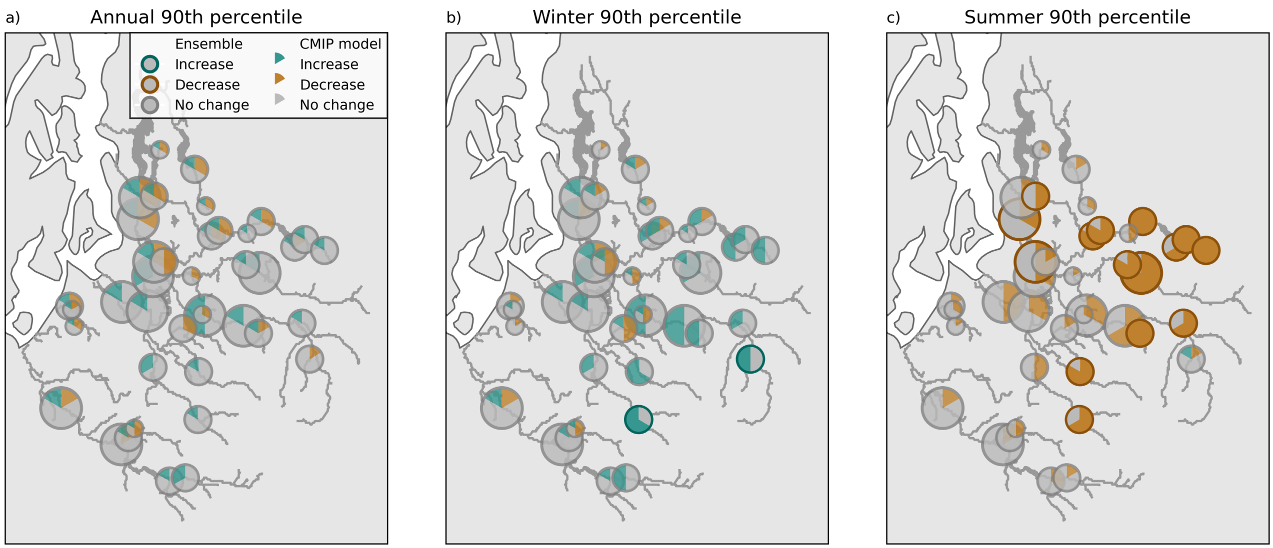

Figure 10. Sign of change in 90th percentile discharge as predicted by the ensemble of climate models (outlines) and the individual CMIP models (pie chart) at USGS streamgage locations. Size of the circle is related to the average observed discharge (e.g., Fig. 5). The six CMIP models build up the pie chart and are sorted by their sign, so the exact location of each CMIP model can change per location/panel. Blue colors indicate an increase, brown colors indicate a decrease, and gray color indicate no clear change. If the ensemble data did not indicate a clear change, the circle and pie chart is made slightly transparent to improve emphasis on locations with a clear change.

not observed in the annual 90th percentile discharge. Interestingly, the relative positions of the climate model runs showed more variability, especially for annual values (Fig. 13a). For example, the HadGemHMsst model showed a negative trend with elevation, while the CNRM and HadGemHM models showed a positive trend. Similarly for winter 90th percentile discharge, the HadGemHMsst model ranged from +20% for lower elevation locations to almost +30% for high elevation locations (based on the smoothed line), while the CNRM (and HadGemHM) model run ranged from +5% (-5%) to +20% (+15%). The relative positions/order of the models were more consistent for the summer values.

4 Discussion

This study provides insight into the projected hydrological changes for the major river basins located in the King and Pierce Counties. However, this is not the first study to investigate the effect of climate change on hydrology in this region. For example, similar to our results, Mantua et al. (2010) found that the summer low discharges are expected to decrease and that the winter period will get more frequent flooding. Lee et al. (2016) found similar trends, with increases in peak discharges and decreases in low discharges. Wu et al. (2012) focused on average annual and summer discharges and noticed a very small increase (0.6%) in the average annual discharge, and a strong decrease in the summer discharges. The decrease in summer discharge is similar to our results, but the increase in annual average discharge is not supported by our results. However, our decreases were only

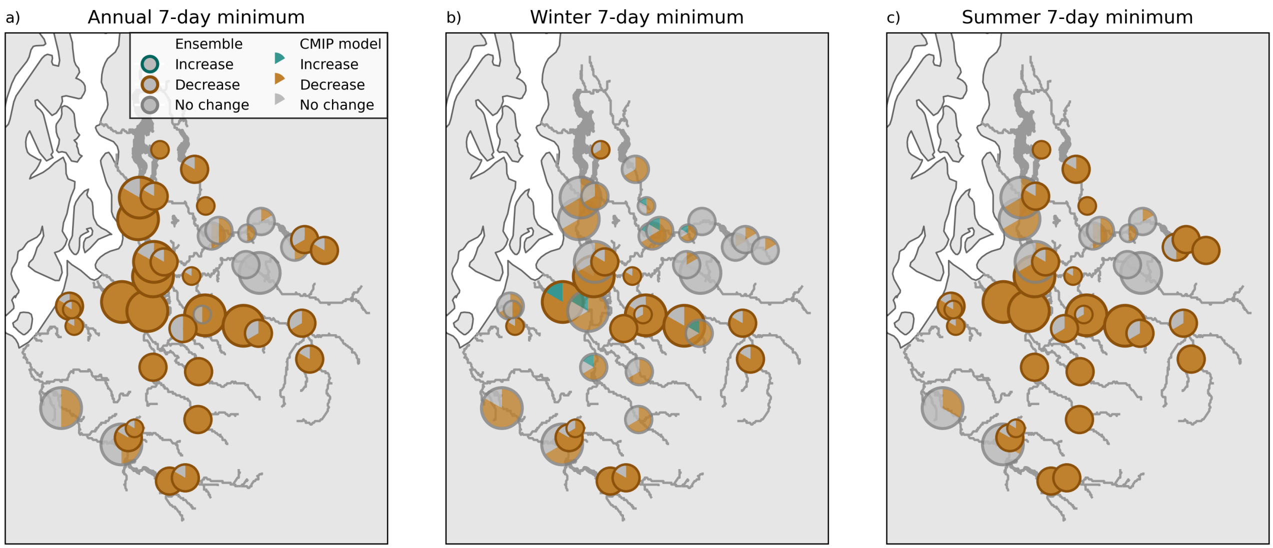

Figure 11. Sign of change in 7-day minimum discharge as predicted by the ensemble of climate models (outlines) and the individual CMIP models (pie chart) at USGS streamgage locations. Size of the circle is related to the average observed discharge (e.g., Fig. 5). The six CMIP models build up the pie chart and are sorted by their sign, so the exact location of each CMIP model can change per location/panel. Blue colors indicate an increase, brown colors indicate a decrease, and gray color indicate no clear change. If the ensemble data did not indicate a clear change, the circle and pie chart is made slightly transparent to improve emphasis on locations with a clear change.

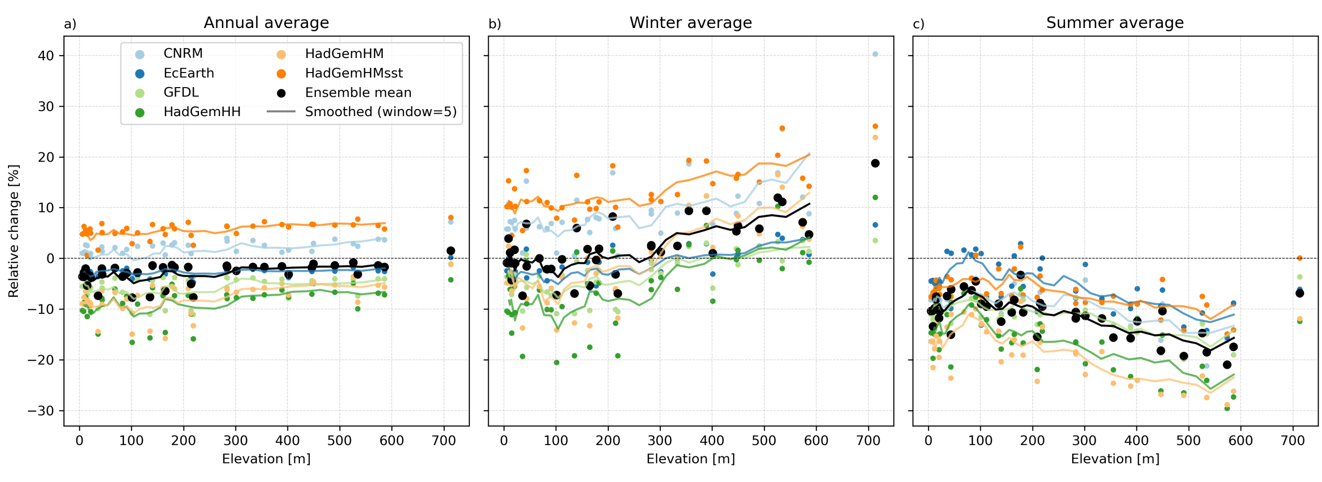

Figure 12. Relation between change in average discharge with elevation (meter above mean sea level), for the ensemble (black circles) and individual climate models (colored circles). Each vertical column of circles indicate a USGS streamgage station. A smoothed line using a rolling mean (with a window of 5 data points) is added to better visualize the response of the climate models. As a result of this window, the smoothed line cannot cover the full extent of the data.

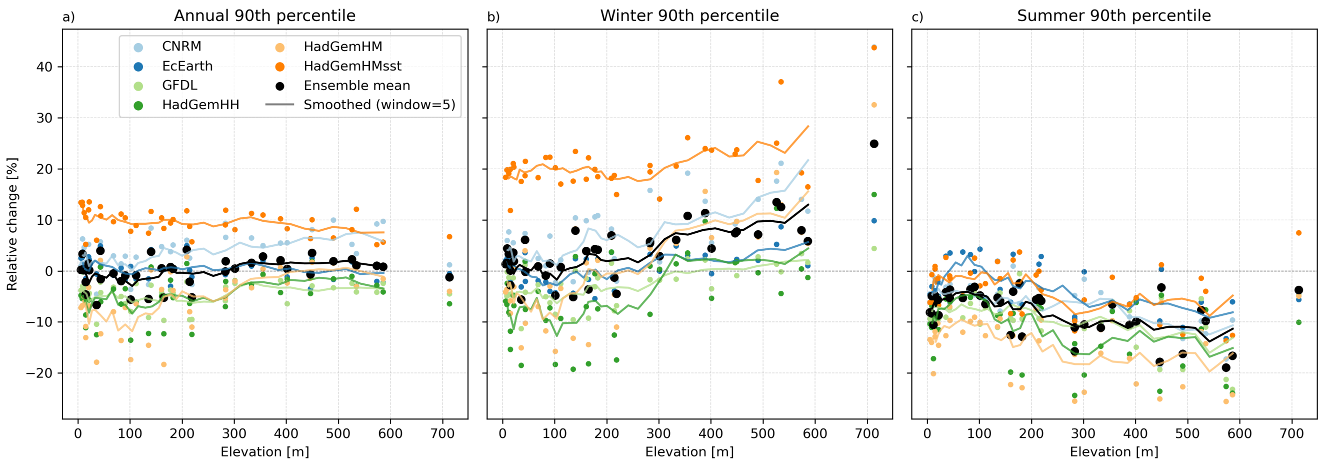

Figure 13. Relation between change in 90th percentile discharge with elevation (meter above mean sea level), for the ensemble (black circles) and individual climate models (colored circles). Each vertical column of circles indicate a USGS streamgage station. A smoothed line using a rolling mean (with a window of 5 data points) is added to better visualize the response of the climate models. As a result of this window, the smoothed line cannot cover the full extent of the data.

minor, and likely rather sensitive to the reference period and specific streamgage location. Multiple studies also describe a shift from a snow-dominated to a rain-dominated river system (Elsner et al., 2010; Mantua et al., 2010; Musselman et al., 2018; Maurer et al., 2018). Although we have not explicitly explored this, our results (increases in winter discharge and decreases in summer discharge) are in line with this regime shift. In contrast, Kormos et al. (2016) showed a high number of locations in the Pacific Northwest that indicated a slight negative trend for average winter discharge, which is opposite to both our results and other literature. However, it should be noted that their study domain covered four states (Washington, Oregon, Montana, and Idaho), while our study only covered a part of the State of Washington. Furthermore, they did not include King and Pierce Counties, which, combined with their larger study area, could explain the differences in results. Their conclusion of a drying trend in summer discharge (both average and low discharges) are consistent with our results and other studies.

Our study also highlights the disagreement between the different CMIP6 models. Where one model might project a clear increase, another model might project a clear decrease. As a result, the ensemble would not be able to distinguish a clear signal from these contrasting responses. This result highlights the importance of including multiple climate models for a more complete analysis. Additionally, we showed that with increasing elevation, and therefore typically also decreasing catchment size, the individual climate models tend to show a more consistent response. As catchments become larger, the hydrological response is driven by more diverse and different processes. A study by Buitink et al. (2017) also showed that contrasting responses within a catchment could be grouped by elevation, and therefore dominant hydrological processes. Chegwidden et al. (2019) also found a large spread between different projections, and showed that higher elevations generally had a smaller spread than mid-elevation regions. They linked this variability in response to changes in the snow pack, which varied strongly with elevation. Similar to our results, Chegwidden et al. (2019) showed that there is good agreement between scenarios projecting a decrease in summer (low) discharges. We hypothesize that further research into the performance and accuracy of the different considered CMIP6 models can help to give more weight to more accurate GCMs and to reduce the spread in the full ensemble. Furthermore, we expect that when a more distant future horizon is also considered, that changes in the hydrological response will become more pronounced.

Musselman et al. (2018) described the importance of rain-on-snow events in driving flood events, and how this importance will change in the future. They describe that rain-on-snow events will become less frequent at lower elevations and more frequent at higher elevations, due to the increasing temperature pushing the front where rainfall is more likely to fall on snowpacks higher up the mountains. They describe that this process, combined with more frequent rainfall as opposed to snowfall due to the increasing temperatures, is likely to cause an increase in flood risk. Because the implemented wflow_sbm model does not support an option to simulate this rain-on-snow processes, it is possible that our annual maxima values are slightly underestimated by not accounting for this process.

Our results are inherently affected by the choice of methodology and the fidelity of input datasets. For example, higher resolution historical meteorological products than the currently used ERA5 reanalysis data are available, especially for precipitation. Using a higher resolution precipitation dataset, would have likely resulted in better model performance throughout the catchment because small-scale processes due to e.g., local orographic effects would likely be better represented in higher resolution data. The performance of the model in small high-elevation basins was found to be worse than at the major outlets (as is visible in Fig. 5). This was mostly attributed to underestimation of discharge (not explicitly shown in this paper), indicating too little precipitation in ERA5 in these regions. Using a higher resolution precipitation product would have likely resulted in better model performance in these regions and all downstream streamgages. However, because our main objective was to use a consistent dataset for model calibration, validation, and bias correction of the climate data, we preferred to use a dataset that had a spatial resolution similar to the CMIP6 climate data. A downside of this is that any errors in the ERA5 data are also indirectly imposed on the climate data via bias correction. However, because the bias correction does not affect the climate signal present in the CMIP6 models, it is unlikely that this choice of using ERA5 substantially affects our conclusions.

As mentioned earlier in the paper, our study area contains several important reservoirs for flood protection and hydropower. Our modeling workflow did not contain any control or feedback mechanisms on how water is released from these reservoirs, but their behavior was determined by analyzing historical inflow and outflow timeseries. With a changing climate, the management strategies of these reservoirs will likely change, thus affecting the downstream locations. Because this is an unknown and a potential source of uncertainty, we decided to keep the reservoir rules constant when simulating the future time horizon.

5 Conclusions

Our study indicates that climate change will substantially alter the hydrological response of the major river basins in King and Pierce Counties, Washington, located in the Pacific Northwest of the United States. Using the physically based, spatially distributed wflow_sbm hydrological model, we simulated river discharge under both historical (1980–2015) and future (2015–2050) climate conditions. The model was carefully calibrated and validated using USGS discharge observations, achieving Kling-Gupta efficiency (KGE) values generally above 0.6 for major river basins. This result provides confidence in the model's ability to represent hydrological processes in the region.

Future climate forcing was derived from individual and an ensemble of six high-resolution CMIP6 models from the High-Resolution Model Intercomparison Project (HighResMIP), which provides 3-hour temporal resolution critical for capturing peak discharges. To reduce systematic biases in temperature and precipitation, climate projections were bias-corrected using the empirical quantile mapping method, with ERA5 reanalysis data as reference.

Results indicate that average river discharges are projected to decrease by approximately 5–10% during summer months and increase by 5-10% during winter. These shifts are primarily driven by rising temperatures, leading to more precipitation falling as rain rather than snow, earlier snowmelt, and increased evapotranspiration. High discharges (90th percentile) are projected to increase during winter by up to ~10%, while low discharges (7-day minimum discharge) may decrease by 20–40%, predominantly in summer. Notably, these changes vary substantially with elevation; higher-elevation basins show more consistent signals across climate models, whereas lowland regions exhibit greater inter-model variability. Variability among individual CMIP6 models often exceeds the ensemble mean climate signal, underscoring substantial uncertainty in future projections, particularly at lower elevations. This highlights the importance of using multi-model ensembles and robust uncertainty assessments in regional climate impact studies.

The modeling framework developed in this study is based on globally available datasets and reproducible calibration procedures and is transferable to other regions for evaluating climate change impacts on river hydrology. Future research could prioritize improving the representation of snow and rain-on-snow processes, refining bias correction techniques for extreme events, and integrating reservoir operation scenarios. Such improvements could help better assess the implications of hydrological changes for water resources management, flood risk mitigation, ecosystem health, and infrastructure planning in the Puget Sound region and beyond.

Data availability. All data supporting the findings are available without restriction in Parker et al. (2025a, b).

Appendix A: Additional results

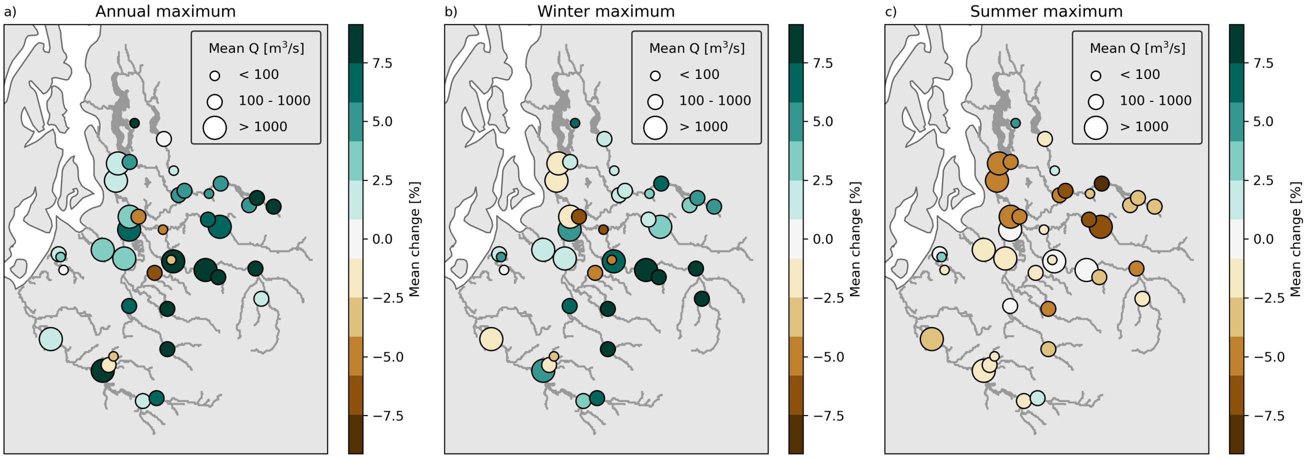

Figure A1. Change in maximum discharge for each USGS station, show for the annual, winter and summer periods (panels a, b, and c, respectively). The colored value represents the mean value of all relative changes from all considered CMIP6 models. The size of the dot indicates the average measured discharge.

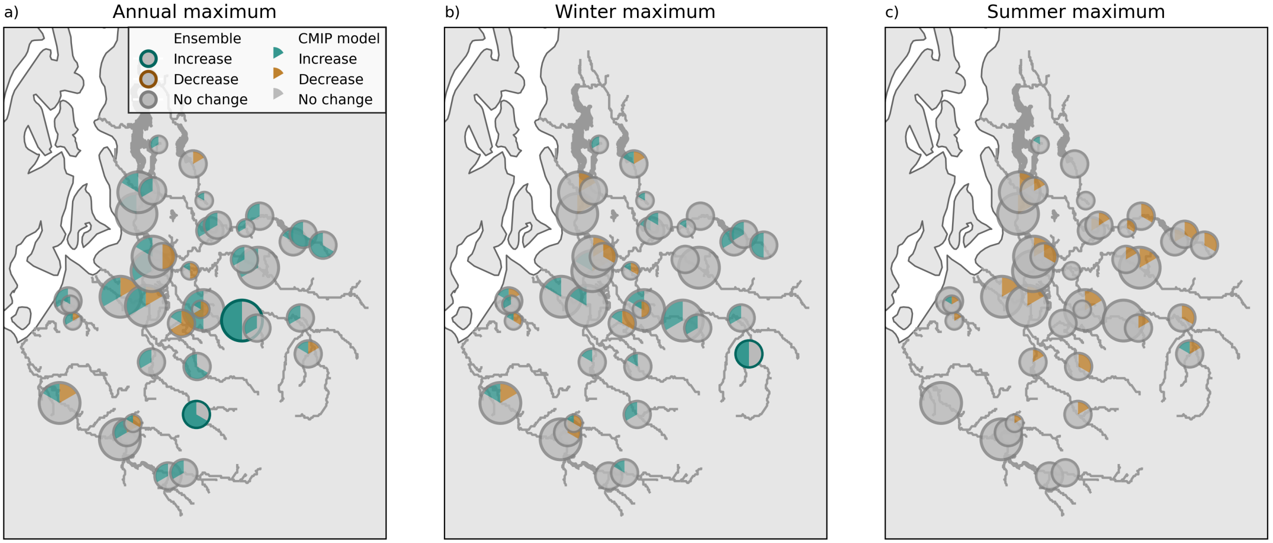

Figure A2. Sign of change in maximum discharge as predicted by the ensemble of climate models (outlines) and the individual CMIP models (pie chart) at USGS streamgage locations. Size of the circle is related to the average observed discharge (e.g., Fig. 5). The six CMIP models build up the pie chart and are sorted by their sign, so the exact location of each CMIP model can change per location/panel. Blue colors indicate an increase, brown colors indicate a decrease, and gray color indicate no clear change. If the ensemble data did not indicate a clear change, the circle and pie chart is made slightly transparent to improve emphasis on locations with a clear change.

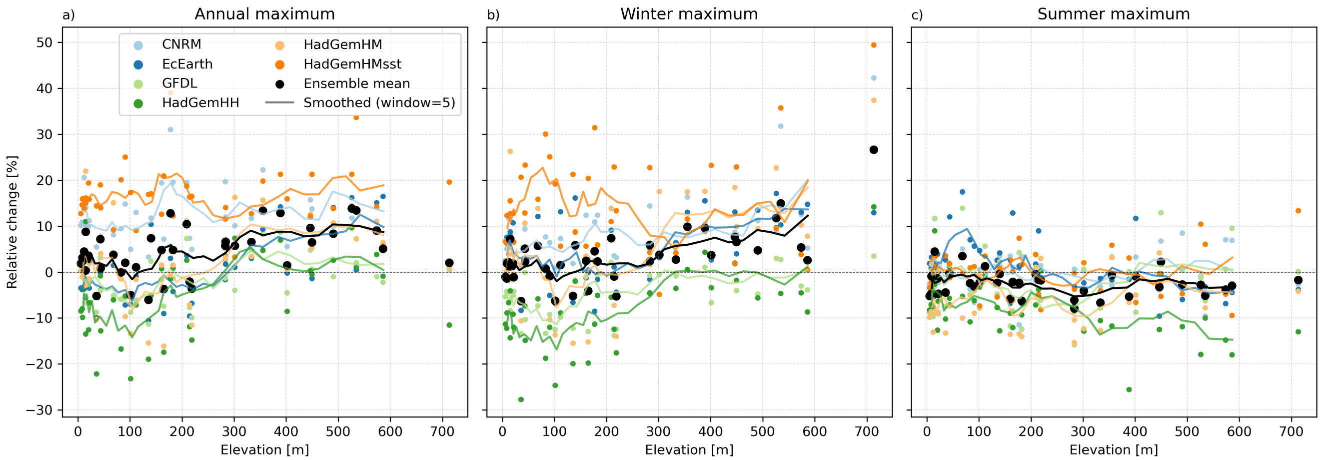

Figure A3. Relation between change in maximum discharge with elevation (meter above mean sea level), for the ensemble (black circles) and individual climate models (colored circles). Each vertical column of circles indicate a USGS streamgage station. A smoothed line using a rolling mean (with a window of 5 data points) is added to better visualize the response of the climate models. As a result of this window, the smoothed line cannot cover the full extent of the data.

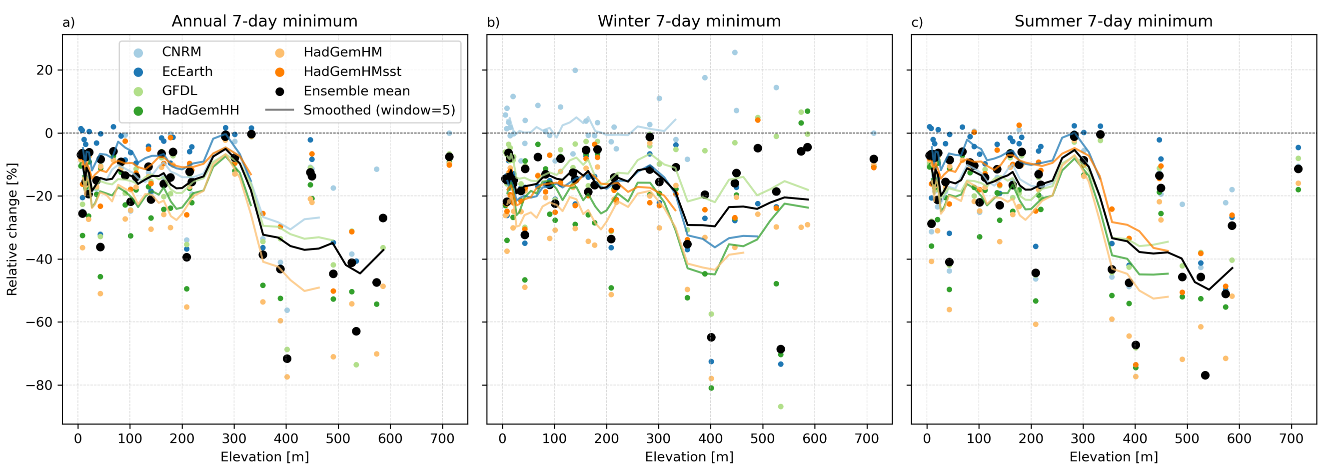

Figure A4. Relation between change in 7-day minimum discharge with elevation (meter above mean sea level), for the ensemble (black circles) and individual climate models (colored circles). Each vertical column of circles indicate a USGS streamgage station. A smoothed line using a rolling mean (with a window of 5 data points) is added to better visualize the response of the climate models. As a result of this window, the smoothed line cannot cover the full extent of the data. Note that some locations experienced very large relative changes due to very small discharge values. These values are removed which causes the smoothed line to stop earlier.

Author contributions. JB, BD, KAP and KN designed the study. JB and BD performed the calibration and hydrological simulations, JB analyzed the results of the climate scenarios and provided the first interpretation of the data. JB and BD wrote the first draft. EG contributed to project conceptualization and was responsible for funding acquisition. All authors contributed to interpreting results, discussing findings, and improving the manuscript.

Competing interests. The authors have no competing interests to declare that are relevant to the content of this article.

Disclaimer. Any use of trade, firm, or product names is for descriptive purposes only and does not imply endorsement by the U.S. Government.

Financial support. The research was funded by the United States Environmental Protection Agency (EPA).

Acknowledgements. We appreciate USGS staff efforts in performing a thorough quality assurance/quality control evaluation of the model results. We also thank Michelle Stern and Anaïs Couasnon for their critical review, which improved the manuscript.

References

Abbass, K., Qasim, M. Z., Song, H., Murshed, M., Mahmood, H., and Younis, I.: A review of the global climate change impacts, adaptation, and sustainable mitigation measures, Environmental science and pollution research, 29, 42 539–42 559, 2022.

Aerts, J. P., Hut, R. W., van de Giesen, N. C., Drost, N., van Verseveld, W. J., Weerts, A. H., and Hazenberg, P.: Large-sample assessment of varying spatial resolution on the streamflow estimates of the wflow_sbm hydrological model, Hydrology and Earth System Sciences, 26, 4407–4430, 2022.

Arino, O., Perez, J. R., Kalogirou, V., Defourny, P., and Achard, F.: GlobCover 2009, ESA Bulletin, https://epic.awi.de/id/eprint/31046/1/Arino_et_al_GlobCover2009-a.pdf, 2009.

Buitink, J., Uijlenhoet, R., and Teuling, A. J.: Hydrological response to climate extremes in mesoscale (pre-) Alpine basins at 0.5° and hyperresolution, Hydrology and Earth System Sciences Discussions, 2017, 1–21, 2017.

Chegwidden, O. S., Nijssen, B., Rupp, D. E., Arnold, J. R., Clark, M. P., Hamman, J. J., Kao, S.-C., Mao, Y., Mizukami, N., Mote, P. W., et al.: How do modeling decisions affect the spread among hydrologic climate change projections? Exploring a large ensemble of simulations across a diversity of hydroclimates, Earth's Future, 7, 623–637, 2019.

Collins, B. D. and Montgomery, D. R.: The legacy of Pleistocene glaciation and the organization of lowland alluvial process domains in the Puget Sound region, Geomorphology, 126, 174–185, 2011.

Cuo, L., Lettenmaier, D. P., Alberti, M., and Richey, J. E.: Effects of a century of land cover and climate change on the hydrology of the Puget Sound basin, Hydrological Processes: An International Journal, 23, 907–933, 2009.

Edmonds, D. A., Caldwell, R. L., Brondizio, E. S., and Siani, S. M.: Coastal flooding will disproportionately impact people on river deltas, Nature communications, 11, 4741, 2020.

Eilander, D., Boisgontier, H., Buitink, J., Couasnon, A., Dalmijn, B., Hegnauer, M., de Jong, T., Loos, S., Marth, I., van Verseveld, W., et al.: HydroMT: Automated and reproducible model building and analysis, Journal of Open Source Software, 8, 4897, 2023.

Eilander, D., Boisgontier, H., van Verseveld, W., Bouaziz, L., Hegnauer, M., Buitink, J., and Dalmijn, B.: hydroMT-wflow, https://doi.org/10.5281/zenodo.14055842, 2024.

Elsner, M. M., Cuo, L., Voisin, N., Deems, J. S., Hamlet, A. F., Vano, J. A., Mickelson, K. E., Lee, S.-Y., and Lettenmaier, D. P.: Implications of 21st century climate change for the hydrology of Washington State, Climatic Change, 102, 225–260, 2010.

Euser, T., Winsemius, H. C., Hrachowitz, M., Fenicia, F., Uhlenbrook, S., and Savenije, H. H. G.: A framework to assess the realism of model structures using hydrological signatures, Hydrology and Earth System Sciences, 17, 1893–1912, https://doi.org/10.5194/hess-17-1893-2013, 2013.

Eyring, V., Bony, S., Meehl, G. A., Senior, C. A., Stevens, B., Stouffer, R. J., and Taylor, K. E.: Overview of the Coupled Model Intercomparison Project Phase 6 (CMIP6) experimental design and organization, Geoscientific Model Development, 9, 1937–1958, 2016.

Fowler, H. J., Ali, H., Allan, R. P., Ban, N., Barbero, R., Berg, P., Blenkinsop, S., Cabi, N. S., Chan, S., Dale, M., et al.: Towards advancing scientific knowledge of climate change impacts on short-duration rainfall extremes, Philosophical Transactions of the Royal Society A, 379, 20190 542, 2021.

Gesch, D., Oimoen, M., Greenlee, S., Nelson, C., Steuck, M., and Tyler, D.: The national elevation dataset, Photogrammetric engineering and remote sensing, 68, 5–32, 2002.

Grossman, E. E., Stevens, A. W., Dartnell, P., George, D., and Finlayson, D.: Sediment export and impacts associated with river delta channelization compound estuary vulnerability to sea-level rise, Skagit River Delta, Washington, USA, Marine Geology, 430, 106 336, 2020.

Grossman, E. E., Crosby, S. C., Stevens, A. W., Nowacki, D. J., Curran, C. A., et al.: Assessment of vulnerabilities and opportunities to restore marsh sediment supply at Nisqually River Delta, west-central Washington, Tech. rep., US Geological Survey, 2022.

Grossman, E. E., Nederhoff, C. M., et al.: Compound flood model for the lower Nooksack River and delta, western Washington—Assessment of vulnerability and nature-based adaptation opportunities to mitigate higher sea level and stream flooding, Tech. rep., US Geological Survey, 2023a.

Grossman, E. E., Tehranirad, B., Nederhoff, C. M., Crosby, S. C., Stevens, A. W., Van Arendonk, N. R., Nowacki, D. J., Erikson, L. H., and Barnard, P. L.: Modeling Extreme Water Levels in the Salish Sea: The Importance of Including Remote Sea Level Anomalies for Application in Hydrodynamic Simulations, Water, 15, 4167, 2023b.

Gupta, H. V., Kling, H., Yilmaz, K. K., and Martinez, G. F.: Decomposition of the mean squared error and NSE performance criteria: Implications for improving hydrological modelling, Journal of hydrology, 377, 80–91, 2009.

Haarsma, R. J., Roberts, M. J., Vidale, P. L., Senior, C. A., Bellucci, A., Bao, Q., Chang, P., Corti, S., Fučkar, N. S., Guemas, V., et al.: High resolution model intercomparison project (HighResMIP v1. 0) for CMIP6, Geoscientific Model Development, 9, 4185–4208, 2016.

Hamlet, A. F., Elsner, M. M., Mauger, G. S., Lee, S.-Y., Tohver, I., and Norheim, R. A.: An overview of the Columbia Basin Climate Change Scenarios Project: Approach, methods, and summary of key results, Atmosphere-ocean, 51, 392–415, 2013.

Hengl, T., Mendes de Jesus, J., Heuvelink, G. B., Ruiperez Gonzalez, M., Kilibarda, M., Blagotić, A., Shangguan, W., Wright, M. N., Geng, X., Bauer-Marschallinger, B., et al.: SoilGrids250m: Global gridded soil information based on machine learning, PLoS one, 12, e0169 748, 2017.

Hersbach, H., Bell, B., Berrisford, P., Biavati, G., Horányi, A., Muñoz Sabater, J., Nicolas, J., Peubey, C., Radu, R., Rozum, I., Schepers, D., Simmons, A., Soci, C., Dee, D., and Thépaut, J.-N.: ERA5 hourly data on single levels from 1940 to present, https://doi.org/10.24381/cds.adbb2d47, accessed on 09-okt-2024, 2023.

Imhoff, R., Van Verseveld, W., Van Osnabrugge, B., and Weerts, A.: Scaling point-scale (pedo) transfer functions to seamless large-domain parameter estimates for high-resolution distributed hydrologic modeling: An example for the Rhine River, Water Resources Research, 56, e2019WR026 807, 2020.

Imhoff, R. O., Buitink, J., van Verseveld, W. J., and Weerts, A. H.: A fast high resolution distributed hydrological model for forecasting, climate scenarios and digital twin applications using wflow_sbm, Environmental Modelling & Software, p. 106099, 2024.

Kormos, P. R., Luce, C. H., Wenger, S. J., and Berghuijs, W. R.: Trends and sensitivities of low streamflow extremes to discharge timing and magnitude in Pacific Northwest mountain streams, Water Resources Research, 52, 4990–5007, 2016.

Kotz, M., Levermann, A., and Wenz, L.: The economic commitment of climate change, Nature, 628, 551–557, 2024.

Lee, S.-Y., Hamlet, A. F., and Grossman, E. E.: Impacts of climate change on regulated streamflow, hydrologic extremes, hydropower production, and sediment discharge in the Skagit River Basin, Northwest Science, 90, 23–43, 2016.

Lehner, B., Liermann, C. R., Revenga, C., Vörösmarty, C., Fekete, B., Crouzet, P., Döll, P., Endejan, M., Frenken, K., Magome, J., et al.: High-resolution mapping of the world's reservoirs and dams for sustainable river-flow management, Frontiers in Ecology and the Environment, 9, 494–502, 2011.

Lehner, F., Nadeem, I., and Formayer, H.: Evaluating quantile-based bias adjustment methods for climate change scenarios, Hydrology and Earth System Sciences Discussions, 2021, 1–26, https://doi.org/10.5194/hess-2021-498, 2021.

Liang, X., Lettenmaier, D. P., Wood, E. F., and Burges, S. J.: A simple hydrologically based model of land surface water and energy fluxes for general circulation models, Journal of Geophysical Research: Atmospheres, 99, 14 415–14 428, 1994.

Lin, P., Pan, M., Allen, G. H., de Frasson, R. P., Zeng, Z., Yamazaki, D., and Wood, E. F.: Global estimates of reach-level bankfull river width leveraging big data geospatial analysis, Geophysical Research Letters, 47, e2019GL086 405, 2020.

Maity, S. S. and Maity, R.: Changing pattern of intensity–duration–frequency relationship of precipitation due to climate change, Water Resources Management, 36, 5371–5399, 2022.

Mantua, N., Tohver, I., and Hamlet, A.: Climate change impacts on streamflow extremes and summertime stream temperature and their possible consequences for freshwater salmon habitat in Washington State, Climatic Change, 102, 187–223, 2010.

Martel, J.-L., Brissette, F. P., Lucas-Picher, P., Troin, M., and Arsenault, R.: Climate change and rainfall intensity–duration–frequency curves: Overview of science and guidelines for adaptation, Journal of Hydrologic Engineering, 26, 03121 001, 2021.

Mass, C. F., Salathé Jr, E. P., Steed, R., and Baars, J.: The mesoscale response to global warming over the Pacific Northwest evaluated using a regional climate model ensemble, Journal of Climate, 35, 2035–2053, 2022.

Mauger, G., Casola, J., Morgan, H., Strauch, R., Jones, B., Curry, B., Busch Isaksen, T., Whitely Binder, L., Krosby, M., and Snover, A.: State of knowledge: Climate change in Puget Sound, Technical Report PB2016103530, National Oceanic and Atmospheric Administration, Environmental Protection Agency, Washington Univ., Seattle, https://ntrl.ntis.gov/NTRL/dashboard/searchResults/titleDetail/PB2016103530.xhtml, nTIS Issue Number 201619, Contract Number EPA-PC-00J303-09, 2015.

Maurer, E. P., Kayser, G., Doyle, L., and Wood, A. W.: Adjusting flood peak frequency changes to account for climate change impacts in the western United States, Journal of Water Resources Planning and Management, 144, 05017 025, 2018.

Merkens, J.-L., Reimann, L., Hinkel, J., and Vafeidis, A. T.: Gridded population projections for the coastal zone under the Shared Socioeconomic Pathways, Global and Planetary Change, 145, 57–66, 2016.

Messager, M. L., Lehner, B., Grill, G., Nedeva, I., and Schmitt, O.: Estimating the volume and age of water stored in global lakes using a geo-statistical approach, Nature communications, 7, 13 603, 2016.

Miller, I. M., Morgan, H., Mauger, G., Newton, T., Weldon, R., Schmidt, D., Welch, M., and Grossman, E.: Projected Sea Level Rise for Washington State: A 2018 Assessment, Tech. rep., Washington Coastal Resilience Project, https://ntrl.ntis.gov/NTRL/dashboard/searchResults/titleDetail/PB2016103530.xhtml, prepared for the Washington Coastal Resilience Project. Updated 07/2019, 2018.

Moscrip, A. L. and Montgomery, D. R.: Urbanization, flood frequency, and Salmon abundance in Puget lowland streams 1, JAWRA Journal of the American Water Resources Association, 33, 1289–1297, 1997.

Musselman, K. N., Lehner, F., Ikeda, K., Clark, M. P., Prein, A. F., Liu, C., Barlage, M., and Rasmussen, R.: Projected increases and shifts in rain-on-snow flood risk over western North America, Nature Climate Change, 8, 808–812, 2018.

Myneni, R., Knyazikhin, Y., and Park, T.: MCD15A3H MODIS/Terra+ Aqua Leaf Area Index/FPAR 4-day L4 Global 500m SIN Grid V006, NASA EOSDIS Land Processes Distributed Active Archive Center [data set], 2015.

National Oceanic and Atmospheric Administration: U.S. Climate Normals 1991-2020: U.S. Link: Daily Climate Normals (1991-2020) https://www.ncei.noaa.gov/metadata/geoportal/rest/metadata/item/gov.noaa.ncdc:C01621/html, https://www.ncei.noaa.gov/access/us-climate-normals/, accessed on: 05/14/2025, 2020.

Nederhoff, K., Leijnse, T. W., Parker, K., Thomas, J., O'Neill, A., van Ormondt, M., McCall, R., Erikson, L., Barnard, P. L., Foxgrover, A., et al.: Tropical or extratropical cyclones: what drives the compound flood hazard, impact, and risk for the United States Southeast Atlantic coast?, Natural Hazards, 120, 8779–8825, 2024.

Nguyen, P. L., Alexander, L. V., Thatcher, M. J., Truong, S. C. H., Isphording, R. N., and McGregor, J. L.: Selecting CMIP6 global climate models (GCMs) for Coordinated Regional Climate Downscaling Experiment (CORDEX) dynamical downscaling over Southeast Asia using a standardised benchmarking framework, Geoscientific Model Development, 17, 7285–7315, https://doi.org/10.5194/gmd-17-7285-2024, 2024.

Nouri, M. and Veysi, S.: CMIP6 multi-model ensemble projection of reference evapotranspiration using machine learning algorithms, Agricultural Water Management, 306, 109 190, https://doi.org/https://doi.org/10.1016/j.agwat.2024.109190, 2024.

Oh, J.-H., Kug, J.-S., An, S.-I., Jin, F.-F., McPhaden, M. J., and Shin, J.: Emergent climate change patterns originating from deep ocean warming in climate mitigation scenarios, Nature Climate Change, 14, 260–266, 2024.

Parker, K., Nederhoff, K., Erikson, L., Hayden, M., Engelstad, A., Barnard, P., and Grossman, E.: CoSMoS (Coastal Storm Modeling System) modeled flood hazards for King County, Washington, U.S. Geological Survey data release, https://doi.org/10.5066/P13HYXKY, 2025a.

Parker, K., Nederhoff, K., Erikson, L., Hayden, M., Engelstad, A., Barnard, P., and Grossman, E.: CoSMoS (Coastal Storm Modeling System) modeled flood hazards for Pierce County, Washington, U.S. Geological Survey data release, https://doi.org/10.5066/P14U7EK2, 2025b.

Pfeffer, W. T., Arendt, A. A., Bliss, A., Bolch, T., Cogley, J. G., Gardner, A. S., Hagen, J.-O., Hock, R., Kaser, G., Kienholz, C., et al.: The Randolph Glacier Inventory: a globally complete inventory of glaciers, Journal of glaciology, 60, 537–552, 2014.

Porter, S. C. and Swanson, T. W.: Radiocarbon age constraints on rates of advance and retreat of the Puget lobe of the Cordilleran ice sheet during the last glaciation, Quaternary Research, 50, 205–213, 1998.

Richardson, D., Bingham, J., Madison, R., and Williams, R.: Water resources of King County, Washington, https://doi.org/10.3133/wsp1852, 1968.

Rosburg, T. T., Nelson, P. A., and Bledsoe, B. P.: Effects of urbanization on flow duration and stream flashiness: a case study of Puget Sound streams, western Washington, USA, JAWRA Journal of the American Water Resources Association, 53, 493–507, 2017.

Salathé Jr, E. P., Mote, P. W., and Wiley, M. W.: Review of scenario selection and downscaling methods for the assessment of climate change impacts on hydrology in the United States Pacific Northwest, International Journal of Climatology: A Journal of the Royal Meteorological Society, 27, 1611–1621, 2007.

Salathé Jr, E. P., Hamlet, A. F., Mass, C. F., Lee, S.-Y., Stumbaugh, M., and Steed, R.: Estimates of twenty-first-century flood risk in the Pacific Northwest based on regional climate model simulations, Journal of Hydrometeorology, 15, 1881–1899, 2014.

Sawicz, K., Wagener, T., Sivapalan, M., Troch, P. A., and Carrillo, G.: Catchment classification: empirical analysis of hydrologic similarity based on catchment function in the eastern USA, Hydrology and Earth System Sciences, 15, 2895–2911, https://doi.org/10.5194/hess-15-2895-2011, 2011.

Shamir, E., Imam, B., Morin, E., Gupta, H. V., and Sorooshian, S.: The role of hydrograph indices in parameter estimation of rainfall–runoff models, Hydrological Processes, 19, 2187–2207, https://doi.org/10.1002/hyp.5676, 2005.

Sorland, S., Schär, C., Lüthi, D., and Kjellström, E.: Bias patterns and climate change signals in GCM-RCM model chains, Environmental Research Letters, 13, https://doi.org/10.1088/1748-9326/aacc77, 2018.

Steyaert, J. C., Condon, L. E., WD Turner, S., and Voisin, N.: ResOpsUS, a dataset of historical reservoir operations in the contiguous United States, Scientific Data, 9, 34, 2022.

U.S. Census Bureau, U. D. o. C.: PROFILE OF GENERAL POPULATION AND HOUSING CHARACTERISTICS, U.S. Census Bureau, https://data.census.gov/table/DECENNIALDP2020.DP1?g=310XX00US42660&d=DEC+Demographic+Profile, accessed on 20 June 2025.

U.S. Geological Survey: USGS Water Data for the Nation: National Water Information System, Accessed on February 14, 2024, https://doi.org/https://doi.org/10.5066/F7P55KJN, 2024.

van der Laan, E., Hazenberg, P., and Weerts, A. H.: Simulation of long-term storage dynamics of headwater reservoirs across the globe using public cloud computing infrastructure, Science of The Total Environment, 931, 172 678, 2024.

Van Verseveld, W. J., Weerts, A. H., Visser, M., Buitink, J., Imhoff, R. O., Boisgontier, H., Bouaziz, L., Eilander, D., Hegnauer, M., Ten Velden, C., et al.: Wflow_sbm v0. 7.3, a spatially distributed hydrological model: from global data to local applications, Geoscientific Model Development, 17, 3199–3234, 2024.

Vertessy, R. A. and Elsenbeer, H.: Distributed modeling of storm flow generation in an Amazonian rain forest catchment: Effects of model parameterization, Water Resources Research, 35, 2173–2187, 1999.

Wahl, T., Jain, S., Bender, J., Meyers, S. D., and Luther, M. E.: Increasing risk of compound flooding from storm surge and rainfall for major US cities, Nature Climate Change, 5, 1093–1097, 2015.

Wigmosta, M. S., Vail, L. W., and Lettenmaier, D. P.: A distributed hydrology-vegetation model for complex terrain, Water resources research, 30, 1665–1679, 1994.

Wu, H., Kimball, J. S., Elsner, M. M., Mantua, N., Adler, R. F., and Stanford, J.: Projected climate change impacts on the hydrology and temperature of Pacific Northwest rivers, Water Resources Research, 48, 2012.

Yan, H., Sun, N., Fullerton, A., and Baerwalde, M.: Greater vulnerability of snowmelt-fed river thermal regimes to a warming climate, Environmental Research Letters, 16, 054 006, 2021.